Article

Not peer-reviewed version

A Novel G88S Mutation in POR Leads to Severe PORD

Maria Natalia Rojas Velazquez [†], Jimena Lopez Dacal [†], Flemming S. Jorgensen, Nora Sanguineti, Katyayani Sharma, Roxana Marino, Natalia Perez Garrido, Elisa Vaiani, Pablo Ramírez, Paula Scaglia, Agustín Izquierdo, Gabriela Sansó, María Gabriela Ropelato, Ignacio Bergadá, Rodolfo A. Rey, Romina P. Grinspon [*], Amit V. Pandey [*]

Posted Date: 7 October 2025

doi: 10.20944/preprints202510.0422.v1

Keywords: adrenal insufficiency; ambiguous genitalia; androgen synthesis defect; PORD; congenital adrenal hyperplasia; CY17A1

 doi:10.20944/preprints202510.0422.v1

Article

A Novel G88S Mutation in POR Leads to Severe PORD

Maria Natalia Rojas Velazquez [1,2,3,†], Jimena Lopez Dacal [4,†], Flemming S. Jorgensen [5], Nora Sanguineti [4], Katyayani Sharma [1,2,3], Roxana Marino [6], Natalia Perez Garrido [6], Elisa Vaiani [6], Pablo Ramírez [6], Paula Scaglia [4,7], Agustín Izquierdo [4,7], Gabriela Sansó [4,7], María Gabriela Ropelato [4,7], Ignacio Bergadá [4], Rodolfo A. Rey [4,7], Romina P. Grinspon [4,*] and Amit V Pandey [1,2,*]

[1] Department of Pediatrics, University Hospital Bern, Bern, Switzerland
[2] Department of Biomedical Research, University of Bern, Bern, Switzerland
[3] Graduate School for Cellular and Biomedical Sciences, University of Bern, Bern, Switzerland
[4] Centro de Investigaciones Endocrinológicas "Dr César Bergadá" (CEDIE), CONICET-FEI-División de Endocrinología, Hospital de Niños Ricardo Gutiérrez, Buenos Aires, Argentina
[5] Department of Drug Design and Pharmacology, University of Copenhagen, DK-2100 Copenhagen, Denmark
[6] Servicio de Endocrinología, Hospital de Pediatría Juan P. Garrahan, Buenos Aires, Argentina
[7] Unidad de Medicina Traslacional, Hospital de Niños Ricardo Gutiérrez, Buenos Aires, Argentina.
* Correspondence: amit.pandey@unibe.ch (R.P.G.); Tel: 0041 31 632 9637 (R.P.G.); rgrinspon@cedie.org.ar (A.V.P.); Tel 54-11-49635930 (A.V.P.)
† These authors contributed equally to this manuscript and should be considered co-first authors.

Abstract

Context: P450 oxidoreductase (POR) deficiency is a rare congenital adrenal hyperplasia with variable severity. The mechanisms of severe mutations and their full metabolic consequences, including drug metabolism, are not fully characterized. **Objective:** To define the clinical, biochemical, and molecular consequences of a novel homozygous *POR* missense mutation, p.Gly88Ser (G88S), identified in four unrelated Argentine families. **Design:** A translational study combining clinical case series analysis with comprehensive in vitro molecular and functional characterization of the novel protein variant. **Setting:** Tertiary pediatric endocrine centers in Argentina and Switzerland. **Patients:** Five individuals (four 46,XY; one 46,XX) from four unrelated families presenting with disorders of sex development and adrenal dysfunction. **Main Outcome Measures:** Clinical phenotypes, hormonal profiles, and *POR* gene sequencing. In vitro analysis of recombinant POR measured flavin content, reductase activity, and support of steroidogenic and drug-metabolizing P450s. **Results:** All patients were homozygous for the c.262G>A (p.G88S) mutation. This FMN-binding domain variant caused protein instability with severe loss of FMN (<30%) and FAD (<15%) cofactors. Steroidogenic activities were virtually abolished (CYP21A2: 1.3%; CYP17A1 17,20-lyase: 5.5% of wild-type), explaining the clinical phenotype. Activities of major drug-metabolizing enzymes were also severely impaired (3-9% of wild-type), establishing a " poor metabolizer" phenotype. **Conclusions:** The *POR* G88S mutation causes one of the most severe forms of PORD described, driven by dynamic protein instability and cofactor loss. It is a critical pharmacogenomic marker, and its recurrence in Argentina suggests a potential screening target.

Keywords: adrenal insufficiency; ambiguous genitalia; androgen synthesis defect; PORD; congenital adrenal hyperplasia; CY17A1

 doi:10.20944/preprints202510.0422.v1

Introduction

POR deficiency (PORD), with OMIM designations 613537 and 201750, is a type of congenital adrenal hyperplasia that was initially discovered in patients exhibiting abnormal steroidogenesis [1,2]. In 2004, we and others described mutations in the Cytochrome P450 oxidoreductase (POR) gene that caused alterations in steroid metabolism [2–6]. Further investigations have revealed that many *POR* mutations result in disorders of sexual development, which are sometimes accompanied by bone malformation [7–11]. POR is crucial for transferring redox equivalents from the reduced form of nicotinamide adenine dinucleotide phosphate (NADPH) to type 2 cytochrome P450 proteins located in the endoplasmic reticulum, which allows them to perform their catalytic functions (Figure 1A) [12–14]. Furthermore, POR has the ability to reduce heme oxygenase, cytochrome b5, and a variety of small molecules and dyes (Figure 1B) [15–23]. POR's involvement in many metabolic processes makes it essential for life, as shown by the fact that POR knockout mice die during embryonic development [24–30]. The wide range of disorders linked to POR deficiency highlights the critical role of POR in various physiological processes. The effect of POR mutations on steroid metabolism can result in a range of endocrine and reproductive issues [31–33]. Additionally, POR's involvement in other metabolic pathways may contribute to the diverse clinical manifestations seen in patients with PORD. To fully explain the complex role of POR in health and disease, and to develop targeted therapies for POR deficiency, further research is required [34,35].

The POR protein is critical to the cytochrome P450 system, as it interacts with 50 different cytochrome P450 proteins [1,36,37]. Due to this extensive network of interactions, it is difficult to accurately predict the consequences of specific POR mutations [38–43]. However, extensive research has shown some trends. Mutations that result in the loss of flavin cofactors (FAD and FMN) within the POR protein have a stronger effect on enzymatic activity [1,44–47]. This loss causes a severe form of POR deficiency that is often lethal. While protein instability is a known pathomechanism for some severe *POR* mutations, the specific molecular dynamics leading to such instability and catastrophic cofactor loss are not fully understood for all variants [32,48,49]. The hinge region of the POR protein is essential for the movement of the FMN and FAD domains [50–55]. Mutations in this region can cause a form of POR deficiency with a wide range of symptoms [48]. The severity and specific manifestations of the disease can depend on which P450 enzymes are involved and the extent to which they are affected. The NADPH binding site is another crucial region of the POR protein. Mutations near this site can disrupt the activity of multiple cytochrome P450 enzymes [31,56]. The specific effects on individual enzymes can differ, leading to a complex array of symptoms and varying disease severity. Overall, *POR* mutations can have a significant effect on the human cytochrome P450 system, resulting in a range of disorders with varying degrees of severity. Due to the complexity of the POR protein's interactions with numerous cytochrome P450 proteins, the specific effects of individual mutations are difficult to predict. However, ongoing research continues to clarify the underlying mechanisms and potential therapeutic targets for POR-related disorders [57].

 doi:10.20944/preprints202510.0422.v1

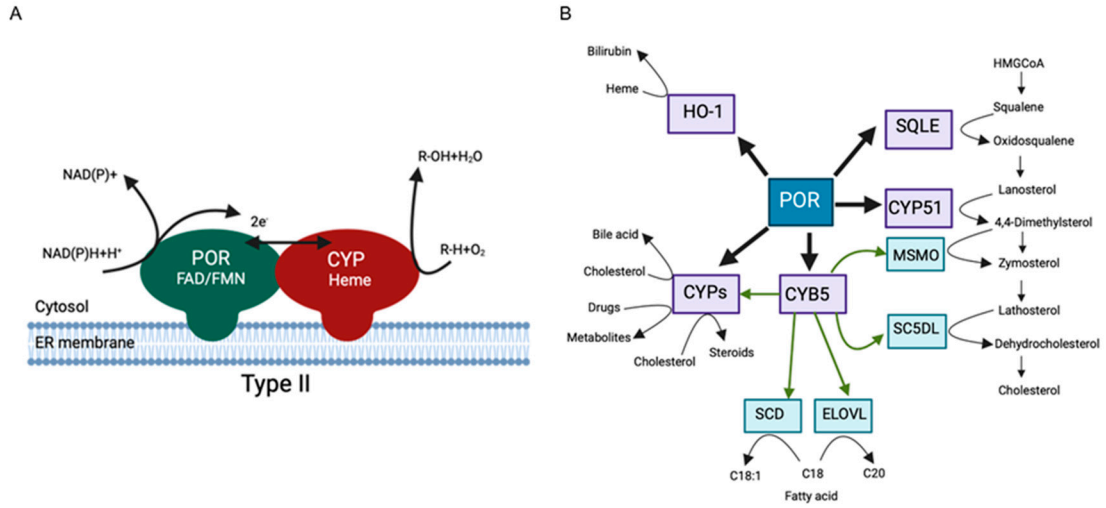

Figure 1. Role of POR in metabolism. A. Schematic representation of electron transfer from P450 oxidoreductase (POR) to a Type II cytochrome P450 (CYP) enzyme in the endoplasmic reticulum (ER) membrane. The FMN domain of POR interacts with a cytochrome P450 (CYP) enzyme, which is also embedded in the ER membrane. **B.** The central role of P450 oxidoreductase (POR) in human metabolic processes. POR is crucial for the activity of several CYPs involved in the synthesis of all steroid hormones, including those of the adrenal cortex (e.g., cortisol, aldosterone, androgens) and the gonads (e.g., estrogens, testosterone). POR supports CYP51 (lanosterol synthase), for the conversion of lanosterol to cholesterol in the cholesterol biosynthesis pathway. POR may also interact with MSMO (methylsterol monooxygenase) in further steps of this pathway. POR is also the obligate electron donor for many hepatic and extrahepatic CYPs, which are responsible for the phase I metabolism of a vast number of drugs, toxins, and other xenobiotic compounds. POR also interacts with Heme Oxygenase-1 (HO-1) in the breakdown of heme, for the formation of bilirubin and in conjunction with Cytochrome b5 (CYB5), provides electrons to enzymes like Stearoyl-CoA Desaturase (SCD) and enzymes involved in the elongation of Very Long-Chain Fatty Acids (ELOVL), which are critical for the synthesis of unsaturated and long-chain fatty acids. Dysfunction of POR, in POR deficiency, can therefore lead to a wide spectrum of clinical manifestations affecting these diverse metabolic pathways. Created by BioRender.com.

In the current study, a recently discovered G88S mutation in POR was investigated. This mutation was identified in several unrelated patients from Argentina who exhibited impaired gonadal and adrenal steroid production. The multiple enzyme activities affected by the G88S mutation in POR were characterized through biochemical analysis of patient samples and the generation of recombinant POR protein incorporating the G88S mutation. We focused on the effects of the G88S mutation on two steroid-metabolizing P450 enzymes, CYP17A1 (17-hydroxylase and 17,20 lyase activities) and CYP21A2 (21-hydroxylase activity) based on biochemical laboratory results and hormonal measurements from patients. We confirmed that the G88S mutation severely impaired CYP17A1 and CYP21A2 activities, which explains the under virilization in 46,XY individuals and the pubertal delay in one 46,XX patient associated with adrenal insufficiency. Furthermore, given that PORD is known to affect drug metabolism, we investigated the quantitative impact of this severe mutation on a broad panel of drug-metabolizing enzymes, an under-investigated area with critical implications for the lifelong clinical management of affected individuals. The direct metabolic activities of POR on small molecules, and a soluble probe substrate cytochrome c were also tested to identify different mechanisms that may affect POR due to the G88S mutation. The experiments revealed two distinct mechanisms for the pathogenicity of the POR G88S mutation: The inhibition of CYP17A1 and CYP21A2 activities and an overall reduction in POR activities due to a loss of flavin content, suggesting protein instability. These findings provide valuable insights into the functional consequences of the G88S mutation in POR and its contribution to the insufficient gonadal and adrenal steroid hormone production in affected individuals. By elucidating the molecular

 doi:10.20944/preprints202510.0422.v1

mechanisms underlying POR-related disorders, this research may facilitate the development of novel diagnostic and therapeutic approaches for patients with POR mutations.

Methods

Study Approval and Patient Consent

The study was conducted in accordance with the Declaration of Helsinki and was approved by the Ethics Review Committee of the Hospital de Niños Ricardo Gutiérrez, Buenos Aires, Argentina. Written informed consent was obtained from the parents or legal guardians of all participants.

Clinical Assessment

Clinical assessments included length and weight measurements expressed as standard deviation scores (SDS) based on the Argentine population reference [58], external genitalia scoring (EGS) [59], pubertal staging according to Marshall and Tanner system [60], and penile size measurement compared to population-specific data of the Argentine population [61].

Hormone Assays: Serum levels of numerous hormones, including follicle-stimulating hormone (FSH), luteinizing hormone (LH), testosterone (T), progesterone (P4), and cortisol, were measured utilizing an electrochemiluminescence assay (ECLIA) on a COBAS e-411 analyzer. This method employs a sandwich test principle for FSH and LH and a competitive principle for T, P4, and cortisol, with an incubation duration of 18 minutes. The World Health Organization (WHO) second IS 80/552 and the WHO second IRP 78/549 served as standards for LH and FSH, respectively. The Cortisol II method by ECLIA has been standardized against the IRMM (Institute for Reference Materials and Measurements)/IFCC-451 panel utilizing isotope dilution-gas chromatography/mass spectrometry (ID-GC/MS). The Elecsys Progesterone III assay is traceable via ID-GC/MS to highly purified progesterone by weight, similar to BCR-348R and ERM-DA347, and the Elecsys Testosterone II assay has been standardized via ID-GC/MS. The sensitivity of the assays for LH and FSH was 0.10 IU/L, and for T, P4, and cortisol was 10 ng/dL, 0.2 ng/mL, and 0.1 µg/dL, respectively. Commercial control materials from Bio-Rad (Lyphochek® Immunoassay Plus) were utilized to determine intra- and between-run precision (CVi% and CVb%, respectively). CVi and CVb were 1.1 and 1.8% for LH and 1.0 and 4.2% for FSH, respectively, and less than 2 and 4%, respectively, for steroid immunoassays.

Dehydroepiandrosterone sulfate (DHEA-S) and adrenocorticotropin (ACTH) were measured in serum utilizing a chemiluminescence assay on the IMMULITE 2000XPi analyzer from Siemens. The sensitivity for DHEA-S and ACTH was 150 ng/mL and 10 pg/mL, with CVi and CVb less than 5 and 7%, respectively. Androstenedione (A) and 17-hydroxyprogesterone (17OHP) concentrations were measured utilizing a current coated-tube competitive commercially available RIA from Diasource (Nivelles, Belgium), with CVi% and CVb% less than 4.5% and 9.0% for A and less than 4.3% and 8.0% for 17OHP [62,63]. In children younger than 1 year old, 17OHP was determined after an organic extraction procedure utilizing diethyl ether [62]. Anti-Müllerian hormone (AMH) was measured utilizing the AMH/MIS ELISA kit (Immunotech-Beckman, Marseilles, France) [64,65]. CVi% and CVb% were 10.5% and 9.4% for a serum AMH concentration of 700 pmol/L and 11.1 and 12.8% for a serum AMH concentration of 7 pmol/L. An ACTH stimulation test (250 µg/m2, maximum 250 µg) was performed. ACTH was measured in serum at time 0, and cortisol, testosterone, androstenedione, 17OHP, and progesterone were measured in serum at 0 and after 60 minutes. A human chorionic gonadotropin (hCG) stimulation test consisted of six injections of 1,500 IU or four injections of 2,500 IU every other day [66]. Testosterone, androstenedione, 17OHP, and progesterone were measured before stimulation and one day after the final injection [67].

Next Generation Sequencing (NGS) and Filtering: Genomic DNA was extracted from peripheral venous blood cells using the Gentra Puregene Blood Kit (Qiagen) according to manufacturer instructions. The DNA was quantified using a high performance microvolume spectrophotometer Nanophotometer® NP60 (Implen Inc.), and DNA concentration was normalized to 10 ng/µL using a fluorometer Qubit® 3.0 (Invitrogen). DNA purity was assessed by measuring the

 doi:10.20944/preprints202510.0422.v1

absorbance ratio 260/280 nm. DNA library preparation and exon capture from the proband were performed using the TruSight One® sequencing panel (Illumina), which provides coverage of 4813 genes associated with known Mendelian genetic disorders (~12 Mb genomic content). The quality of genomic DNA fragmentation was evaluated using a capillary system Fragment Analyzer™ (Advanced Analytical). NGS by synthesis with fluorescent reversible terminator deoxyribonucleotides was performed using a NextSeq 500® system (Illumina) at the Translational Medicine Unit of the Buenos Aires Children's Hospital (Unidad de Medicina Traslacional, Hospital de Niños Ricardo Gutiérrez, Buenos Aires).

We used the strategy recommended by the Broad Institute in the Genome Analysis Toolkit (GATK best practices™) for preprocessing, variant calling, and refinement. Raw sequence data were mapped to the 1000-Genomes phase II reference genome (GRCh37 version hs37d5) using the BWA-MEM algorithm of Burrows-Wheeler Aligner software [68] and visualized with the Integrative Genomics Viewer (IGV v.2.12.3), Broad Institute and the Regents of the University of California Broad Institute of Massachusetts Institute of Technology and Harvard, Cambridge, Massachusetts, USA (14). Duplicates were removed using Picard (Broad Institute). The variant call format file (VCF) was annotated following ANNOVAR protocol [69] with the following databases: ClinVar (https://www.ncbi.nlm.nih.gov/clinvar/) [70], gnomAD (https://gnomad.broadinstitute.org/) [68], dbSNP (https://www.ncbi.nlm.nih.gov/snp/) [71], GWAS Catalog (https://www.ebi.ac.uk/gwas/) [72], InterVar (https://wintervar.wglab.org/) [69], among others. Copy number variants were evaluated using DECoN algorithm prediction [73].

Variant filtering and prioritization were performed on B_platform (https://www.bitgenia.com/b-platform/). Candidate gene list, according to the patient's 46,XY DSD phenotype, included the following genes: *AKR1C2, AKR1C4, ARX, ATRX, CDKN1C, CYB5A, CYP11B1, CYP17A1, CYP19A1, CYP21A2, DHCR7, ESR1, FGFR2, HSD17B3, HSD17B4, HSD3B2, LHCGR, NR3C1, POR, SRD5A2, STAR*. Single nucleotide variants (SNVs) and indels fulfilling the following criteria were considered for further analysis and a more detailed manual curation: read depth ≥10X, and Genotype Quality (GQ) score ≥45, minor allele frequency (MAF) <1% in gnomAD exomes and genomes and in 1000 Genomes databases and in our own in-house database including over 800 Argentine pediatric patients. Considering the evidence available, variants were classified according to their potential pathogenicity using the American College of Medical Genetics and Genomics (ACMG) guidelines for variant interpretation [69] following the ClinGen Sequence Variant Interpretation working group recommendations (https://www.clinicalgenome.org/working-groups/sequence-variant-interpretation/).

Sanger Sequencing: Genomic DNA was isolated from peripheral blood leukocytes by conventional methods. The entire coding region (exons 1-15) and splice sites in flanking intronic regions of POR gene were polymerase chain reaction (PCR) amplified and sequenced by automated analyzer. Following PCR, the products were assessed by electrophoresis on a 1% agarose gel stained with ethidium bromide and showing a single band with expected size. The PCR products were purified (Qia Quick PCR Purification Kit, Qiagen, Buenos Aires, Argentina) and sequenced using a BigDye Terminator version 3.1 cycle sequencing kit (Applied Biosystems, Buenos Aires, Argentina) on an ABI PRISM® 3130 Genetic Analyzer capillary DNA sequencer (Applied Biosystems, Buenos Aires, Argentina). The primers used for sequencing were the same as those used for PCR and are listed in Supplementary Table 1. Previously reported intronic mutations were also analyzed [Human Gene Mutation Database (HGMD), www.hgmd.cf.ac.uk/]. The nucleotide sequences obtained were compared with the NCBI entries of POR gene (NG_008930.1) using SeqScape software v0.2.6 (Applied Biosystems). Nucleotide changes were reconfirmed in each sample DNA by antisense sequence and resequencing after a new PCR product was produced from the original DNA extract.

Table 1. Hormonal values in index patients 1 to 4 with POR deficiency. 17OHP: 17-hydroxyprogesterone, A4: Androstenedione, ACTH: adrenocorticotropic hormone, AMH: Anti-Müllerian hormone, DHEA-S: dehydroepiandrosterone-sulfate, FSH: follicle-stimulating hormone, LH: luteinizing hormone, T: testosterone.

 doi:10.20944/preprints202510.0422.v1

	Patient 1				Patient 2				Patient 3		Patient 4			
Age	**3 months**		**6 months**		**12 yr**		**12 yr**		**10 yr**		**8 months**		**11 months**	
Hormonal test	basal	Post hCG	basal	Post ACTH	basal	Post hCG	basal	Post ACTH	basal	Post ACTH	basal	Post hCG	basal	Post ACTH
T ng/dL	**18**	**54**	-	-	**<10**	**156**	<10	-	<20		**40**	**95**	<10	<10
A4 ng/dL	-	16	19	49	21	23	21	26	<10	<10	51	11	21	17
17OHP ng/mL	7.9	6.1	**19.5**	**19.4**	12.7	9.8	**12.7**	**15**	**17.6**	**16.6**	9.6	9.6	**11.9**	**14.5**
Progesterone ng/mL	21	25	**26**	**> 66**	20.5	10.7	**20.5**	**26.3**	**34**	**> 66**	**-**	**-**	**> 66**	**> 66**
DHEA-S ng/mL					591	304	591	588	<20		<150	<150	<150	<150
ACTH pg/mL	-	-	**84**	-	-	-	**72**	-	**129**		-	**-**	**413**	-
Cortisol µg/dL	-	-	**11.1**	**11.1**	-	-	**9.3**	**8.5**	**5.7**	**4.7**	**-**	**-**	**8.3**	**8.5**
AMH pmol/L	385				496	-	-	-	162		1328	-	-	-
LH IU/L	0.3	-	-	-	1.6	-	-	-	0.6		5.2	-	-	-
FSH IU/L	1.1	-	-	-	1.4	-	-	-	5.8		1.8	-	-	-

Expression of POR proteins in bacteria and membrane purification: The human POR WT and G88S mutant proteins (NCBI# NP_000932, Uniprot# P16435) were expressed in bacteria utilizing a heterologous gene expression protocol. Recombinant POR variants (N-23 form) were expressed, and bacterial membranes were purified based on previous publications [8,32,74,75] with slight modifications. In brief, pET15b plasmids containing cDNAs for WT or mutant POR were procured from Genscript and employed to transform *E. coli* BL21(DE3) cells. Single colonies were selected and cultivated on carbenicillin plates. The primary shake flask culture utilized autoinduction media comprising terrific broth, 40 mM $FeCl_3$, 4 mM $ZnCl_2$, 2 mM $CoCl_2$, 2 mM Na_2MoO_4, 2 mM $CaCl_2$, 2 mM $CuCl_2$, 2 mM H_3BO_3, 0.5 mg/ml riboflavin, and 100 µg/ml carbenicillin. Cells were grown at 37 °C to an OD_{600} of 0.6, then the temperature was decreased to 25 °C for 16 h.

The bacterial cells were collected via centrifugation, washed with PBS, and gently stirred for 1 h at 4 °C in 50 mM Tris-acetate (pH 7.6), 0.25 M sucrose, 0.5 mM EDTA, lysozyme (0.2 mg/ml), 1 mM PMSF, and 20 U/ml endonuclease to prepare spheroplasts. The spheroplasts were collected through centrifugation at 5000 x g for 20 min and resuspended in 50 mM potassium phosphate (pH 7.6) containing 6 mM Magnesium acetate, 0.1 mM DTT, 20% (v/v) glycerol, and 1 mM PMSF; and disrupted by sonication. Following centrifugation at 12000 × g for 15 min at 4 °C, the supernatant was

 doi:10.20944/preprints202510.0422.v1

centrifuged at 100000 × g for 90 min at 4 °C to collect membranes. Purified membranes containing POR were resuspended in 50 mM Potassium phosphate buffer (pH 7.8) and 20% (v/v) glycerol and stored at −70 °C. Protein concentration was quantified by the RC-DC protein assay (Bio-Rad), and POR content was quantified by western blot analysis.

His6-Tag protein-containing isolated membranes were solubilized in a solution of 50 mM Potassium Phosphate, pH 7.4, 10% (v/v) glycerol, and 1% Triton X-100, at a concentration of 0.25 g of membrane per mL of solution. The mixture was gently stirred for 16 hours and then centrifuged at 12,000 ×g for 15 minutes. The resulting supernatant was diluted with buffer A to a final concentration of 50 mM potassium phosphate, pH 7.4, 30 mM imidazole, 0.1% Triton, 150 mM NaCl, and 10% glycerol, and then used for purification by ion-metal affinity chromatography (IMAC). The diluted supernatant was loaded into 4 mL His60 Ni Superflow™ Resin. Impurities were washed out with buffer A, with an increased imidazole concentration to 60 mM. The tagged proteins were eluted using the same buffer with imidazole concentrations up to 500 mM, and the presence of POR was confirmed by Western blot. The purified samples were concentrated, and the elution buffer was exchanged for 50 mM Potassium Phosphate, pH 7.4, 10% (v/v) glycerol, and 0.1% Triton X-100 using Amicon® Ultra Centrifugal Filters 20,000 MWCO. The final protein concentration was measured using the Pierce™ Coomassie Plus Assay Kit (ThermoFisher Scientific), following the manufacturer's instructions.

Western Blot Analysis to Determine POR Content in Membranes: Western blot analysis was conducted to determine POR content in membranes as described previously [31,76]. In short, 1 µg of bacterial membrane proteins were separated on an SDS-PAGE gel and blotted onto polyvinyl difluoride (PVDF) membranes. The blots were first incubated with a rabbit polyclonal antibody against POR-WT from Genscript (Genscript, NJ, USA) at a 1:1000 dilution. Then, a secondary goat anti-rabbit antibody labeled with an infrared dye (IRDye 680RD, LI-COR Bioscience Inc., NE, USA) was used at a 1:15000 dilution. An Odyssey Infrared Imaging System (LI-COR Bioscience Inc., NE, USA) was used to analyze signals with the 700 nm fluorescent channel, and protein bands were quantitated using the Odyssey software (LI-COR Bioscience Inc., NE, USA). Purified wild-type POR was used as a standard for normalizing the POR content of each membrane preparation. The normalized amount of POR content was used for POR-WT and POR-G88S protein in all the experiments described here.

Small Molecule Reduction Assay by POR-WT and POR-G88S

Cytochrome C Assay: To evaluate cytochrome c reduction activity, triplicate reactions were conducted in a 96-well plate using a microplate reader. The reaction mixture comprised 50 nM POR in 50 mM Tris-HCl buffer (pH 7.8) with 150 mM NaCl. Varied concentrations of cytochrome c (ranging from 2.5 to 60 µM) were added to the reaction mixture. The reaction was initiated by introducing 100 µM NADPH, and the absorbance at 550 nm was monitored for 10 minutes; measurements were performed using a Spectramax M2e plate reader (Molecular Devices, Sunnyvale, CA, USA). Reaction rates were determined by calculating the slope from the linear range of the kinetic traces. Vmax and Km values were obtained by fitting the data to the Michaelis-Menten equation [32,34].

NADPH-dependent MTT Assay: For the NADPH-dependent MTT (3-(4,5-Dimethylthiazol-2-yl)-2,5-diphenyltetrazolium bromide) assay, the reaction mixture contained 50 nM POR in 50 mM Tris-HCl buffer (pH 7.8) with 150 mM NaCl. Varied concentrations of MTT (ranging from 3.9 to 500 µM) were included in the reaction mixture. The reaction was initiated by adding 100 µM NADPH, and the rate of increase in absorbance at 610 nm was measured for 30 minutes using the extinction coefficient ($\varepsilon 610 = 11\ mM^{-1}\ cm^{-1}$); measurements were performed using a Spectramax M2e plate reader (Molecular Devices, Sunnyvale, CA, USA). Reaction rates were determined by calculating the slope from the linear range of the kinetic traces. Vmax and Km values were obtained by fitting the data to the Michaelis-Menten equation [32,34].

NADPH-dependent Resazurin Reduction Assay: To assess the reduction activity of POR, a NADPH-dependent Resazurin (RS) reduction assay was performed. The reaction mixture consisted

 doi:10.20944/preprints202510.0422.v1

of 100 nM POR in 50 mM Tris-HCl buffer (pH 7.8) with 150 mM NaCl. Varied concentrations of Resazurin were added to the reaction mixture (ranging from 2.5 to 20 μM). The reaction was initiated by the addition of 100 μM NADPH, and the rate of increase in emission (570 nm excitation, 585 nm emission for RS) was measured using the corresponding extinction coefficient ($\varepsilon\lambda$ = 60 mM^{-1} cm^{-1}). The reaction progress was monitored for 30 minutes, and the emission data were recorded using a Spectramax M2e plate reader (Molecular Devices, Sunnyvale, CA, USA). Reaction rates were determined by calculating the slope from the linear range of the kinetic traces. Vmax and Km values were obtained by fitting the data to the Michaelis-Menten equation [32,34].

Flavin Content Analysis of WT and Mutant POR: To determine the flavin content of the protein samples, the samples were first treated with 2 M urea for 1 hour to release the flavin molecules from the protein structure. The solution was then centrifuged at 13,000 rpm for 10 minutes to remove any precipitated proteins. The fluorescence intensity of the released flavin molecules, Flavin mononucleotide (FMN) and Flavin adenine dinucleotide (FAD), was then measured separately at pH 7.7 and pH 2.6, respectively, with excitation at 450 nm and emission at 535 nm [77].

Assay of CYP17A1 activities: The 17α-hydroxylase of CYP17A1 was assayed using [^{14}C]-progesterone as the substrate [2,8,78,79]. Reactions were performed in 1.5 ml Eppendorf tubes in a final volume of 200 μL at 37° C. The reconstituted liposome system consisted of pure wild-type/mutant POR, purified CYP17A1 (obtained from CYPEX, Dundee, Scotland, UK), and cytochrome b_5 in a ratio of 4:1:1. The final assay mixture was composed of 20 μM DLPC (1,2-Dilauroyl-sn-glycero-3-phosphocholine)/DLPG (1,2-Dilauroyl-sn-glycero-3-phosphoglycerol), proteins (100 nM POR, 25 nM CYP17A1, 25 nM b_5), 10 mM $MgCl_2$, 6 mM KOAc, 1 mM GHS, 1 μM progesterone, and 10,000 cpm [^{14}C]-progesterone in 50 mM Tris-HCl buffer with a pH of 7.4. Reactions were initiated by adding 1 mM NADPH and were stopped with ethyl acetate:isooctane (3:1). Steroids were extracted, separated by TLC (silica gel 60 F-254 TLC plates, Merck) using ethyl acetate:chloroform (3:1) as the solvent system, and quantified by phosphorimaging [8,32,74,75].

The ability of POR to support 17, 20-lyase activity was assayed with liposomes containing human CYP17A1 and wild-type or mutant human POR as the electron donor. CYP17A1 activity was measured by the release of tritiated water from [21-^{3}H]-17-OH-pregnenolone substrate as described [32,34,38,80–83]. Reactions were performed in 1.5 ml Eppendorf tubes in a final volume of 200 μL at 37° C. The reconstituted liposome system consisted of pure wild-type/mutant POR, purified CYP17A1 (obtained from CYPEX, Dundee, Scotland, UK) and cytochrome b_5 in a ratio of 4:1:1. The final assay mixture was composed of 20 μM DLPC (1,2-Dilauroyl-sn-glycero-3-phosphocholine)/DLPG (1,2-Dilauroyl-sn-glycero-3-phosphoglycerol), proteins (100 nM POR, 25 nM CYP17A1, 25 nM b_5), 10 mM $MgCl_2$, 6 mM KOAc, 1 mM GHS, 1 μM 17-OH-pregnenolone, and 40,000 cpm [21-^{3}H]-17-OH-pregnenolone in 50 mM Tris-HCl buffer with a pH of 7.4. Reactions were initiated by adding 1 mM NADPH and were stopped by adding 1 ml of chloroform. The mixture was vortexed for 30 seconds, then 1 ml of water was added, and the mixture was centrifuged at 1,000 rpm for 5 minutes. Aliquots of the water phase (0.5 ml) were taken and mixed with an equal volume of 5% charcoal/0.5% dextran. After 40 seconds of extraction, samples were centrifuged at 12,000 rpm for 15 minutes, and 0.5 ml aliquots of supernatants were collected for counting of ^{3}H radioactivity. The measured cpm values were corrected for background radioactivity and multiplied by a factor of 4 because the actual counted aliquots represented only one-fourth of the total reaction volume.

Assay of CYP21A2 activity: The 21-hydroxylase of CYP21A2 was assayed using [^{14}C]-progesterone as the substrate [84–87]. Reactions were performed in 1.5 ml Eppendorf tubes in a final volume of 200 μL at 37° C. The reconstituted liposome system consisted of pure wild-type/G88S POR and purified CYP21A2 (obtained from CYPEX, Dundee, Scotland, UK). The final assay mixture was composed of 20 μM DLPC (1,2-Dilauroyl-sn-glycero-3-phosphocholine)/DLPG (1,2-Dilauroyl-sn-glycero-3-phosphoglycerol), proteins (100 nM POR, 25 nM CYP21A2), 10 mM $MgCl_2$, 6 mM KOAc, 1 mM GHS, 1 μM progesterone, and 10,000 cpm [^{14}C]-progesterone in 50 mM Tris-HCl buffer with a pH of 7.4. Reactions were initiated by adding 1 mM NADPH and were stopped with ethyl acetate:isooctane (3:1). Steroids were extracted, separated by TLC (silica gel 60 F-254 TLC plates,

 doi:10.20944/preprints202510.0422.v1

Merck) using ethyl acetate:chloroform (3:1) as the solvent system, and quantified by phosphorimaging.

Assay of CYP2C9, CYP2C19, CYP3A4, and CYP3A5 activities: The activities of CYP2C9, CYP2C19, CYP3A4, and CYP3A5 supported by wild-type (WT) or mutant POR were assessed using an in vitro reconstituted system [31,38,48,56,88–91]. For CYP2C9, the reconstituted system comprised bacterial membranes containing WT/G88S POR, purified CYP2C9, and purified cytochrome b5 at a ratio of 5:1:1. The fluorogenic compound BOMCC was utilized as a substrate. The assay mixture consisted of 5 μg DLPC, 3 mM MgCl2, and 20 μM BOMCC in 100 mM Tris-HCl buffer (pH 7.4). 1 mM NADPH was added to initiate the reaction, and fluorescence was measured at an excitation wavelength of 415 nm and an emission wavelength of 460 nm for BOMCC. For CYP2C19, the in vitro CYP2C19 assays were conducted using a reconstituted system consisting of WT/POR-G88S, CYP2C19, and cytochrome b5 at a ratio of 5:1:1. The assay mixture consisted of 2.5 μg DLPC, 3 mM MgCl2, and 20 μM EOMCC in 100 μL of 100 mM Tris-HCl buffer (pH 7.4). The reaction was initiated by the addition of 0.5 mM NADPH, and fluorescence was measured at an excitation wavelength of 415 nm and an emission wavelength of 460 nm for EOMCC. For CYP3A4, an in vitro reconstituted system was employed by mixing POR (WT or G88S), purified CYP3A4, and cytochrome b5 at a ratio of 5:1:1. The final assay mixture consisted of 3 mM MgCl2, 5 μg DLPC, and 20 μM BOMCC in 100 μL of 100 mM Tris-HCl buffer (pH 7.4). 1 mM NADPH was added to initiate the reaction, and the progression of the reaction was monitored by a fluorescence spectrophotometer with sample excitation at 415 nm and emission at 460 nm. For CYP3A5, the in vitro reconstituted system was utilized as described above. The purified CYP3A5, WT/mutant POR, and cytochrome b5 were mixed at a ratio of 1:5:1. The assay mixture consisted of 5 μg DLPC, 3 mM MgCl2, and 20 μM BOMCC in 100 mM Tris-HCl buffer (pH 7.4), and the reaction was initiated by the addition of NADPH to 1 mM final concentration. Fluorescence was monitored for 1 hour. All assays utilized a Spectramax M2e plate reader to measure fluorescence, and all reactions were initiated by the addition of NADPH. The specific substrate and protein ratios varied depending on the CYP enzyme being tested.

Molecular modeling: Structures of the closed conformation of the human POR (PDB 3QE2) and open conformation of the rat POR (PDB 3ES9) were extracted from the Protein Data Bank [92,93]. The glycine to serine mutations were done in Maestro using the Mutate Residues procedure (https://www.schrodinger.com/platform/products/maestro/). All structures were prepared for the MD simulations using the Protein Preparation Procedure in Maestro. MD simulations were performed by the Desmond program accessed from Maestro and applying the default setup procedure. The POR closed conformations were simulated for 100 ns, the FMN domains were simulated for 500 ns, for both systems 100 frames were collected and analysed. Figures of structures were prepared in Pymol.

Statistical analysis–The data were presented as mean and standard error of the mean (SEM). A Student's t-test was used to analyze the differences within experimental subsets; p-values less than 0.05 were considered to be statistically significant.

Results

Case Reports

Patient 1 was referred at 2 months of life for ambiguous genitalia. Parents were reportedly nonconsanguineous of mixed European-Argentine origin, and there was no remarkable family history. The patient was born at 39 weeks with appropriate weight for gestational age and presented imperforate anus and colo-vesical fistula that required early surgical repair. The patient had been assigned male. External genital score (EGS) was 9/12, with phallus of 0.5 cm long and 1 cm wide, distal urethral meatus and fused labioscrotal folds with bilateral palpable gonads. No skeletal features of Antley-Bixler syndrome were observed. Blood pressure was normal. Karyotype was 46,XY. No Müllerian ducts were present on ultrasonography. At 2 months of age, basal testosterone was low (18 ng/dl, ref 180-270), with normal LH (0.25 U/L, ref 0.20-4.20) and FSH (3.8 U/L, ref 0.3-

 doi:10.20944/preprints202510.0422.v1

4.7). AMH was within normal male reference (385 pmol/L, ref 242-1583). At 3 months, Leydig cell testosterone secretion in response to hCG (4 x 2,500 IU) was insufficient (Table 1).

At 6 months, basal ACTH level was elevated with normal cortisol and high 17OHP and progesterone, whereas cortisol showed no response to ACTH stimulus. Altogether these observations were indicative of impaired CYP17A1 and CYP21A2 activities. With the presumptive diagnosis of 46,XY DSD due to a disorder of androgen synthesis, next-generation sequencing was performed (see below). At the age of 13 years, the patients showed clear signs of primary hypogonadism: LH (18.9 IU/L) and FSH (10.1 IU/L) were high while testosterone was undetectable (<10 ng/dl). Additionally, he presented developmental delay and obesity. He did not require corticosteroid replacement but antistress guidelines were provided (Table 2).

Table 2. Patient Clinical Profiles. A quick overview of the key clinical features of the patients with the homozygous G88S mutation in the *POR* gene.

Patient	Age at Presentation	Karyotype	Clinical Features (DSD, Puberty Status, Adrenal Symptoms)	Associated Malformations
Patient 1	2 months	46,XY	Ambiguous genitalia (EGS 9/12), imperforate anus, colo-vesical fistula. At 13 years: primary hypogonadism, developmental delay, obesity.	No skeletal features of Antley-Bixler Syndrome (ABS) observed.
Patient 2	18 days	46,XY	Ambiguous genitalia (EGS 7/12), perineal hypospadias. At 12 years: no clinical signs of puberty. Requires sex steroid and corticosteroid replacement.	No skeletal features of ABS; normal bone X-ray imaging.
Patient 2's Sister	12.5 years	46,XX	Delayed puberty (Tanner B2 breast). Requires sex steroid hormone replacement.	Not reported.
Patient 3	9 years	46,XY	Prepubertal (Tanner B1, PH1), undervirilized genitalia (clitoris <1 cm). Requires hydrocortisone and sex steroid replacement.	Arachnodactyly, thoracic kyphosis, unilateral kidney agenesis, dysmorphic facial features (bulbous nose, flat nasal bridge) consistent with ABS.
Patient 4	5 days	46,XY	Ambiguous genitalia (EGS 4.5/12), perineoscrotal hypospadias. Adequately responded to testosterone administration.	Bulbous nose, left preauricular skin tags. No skeletal features of ABS.

Patient 2, born at 39 weeks with appropriate weight and height for gestational age, was referred at 18 days of life for ambiguous genitalia. Parents reported an absence of consanguinity; the origin of both families was from Argentina. There was no significant family history. EGS was 7/12: the phallus was 1 cm long and 0.6 cm wide, and perineal hypospadias and fused labioscrotal folds with 3-mL

 doi:10.20944/preprints202510.0422.v1

palpable gonads were observed. Blood pressure was normal. Karyotype was 46,XY. No Müllerian ducts were present on ultrasonography. Neonatal screening revealed a slightly elevated 17OHP concentration, which was confirmed in serum after organic extraction (22.1 ng/mL, ref <3.8 ng/mL). However, the 17OHP concentration decreased to normal levels (2.5 ng/mL) by 45 days of life and remained within the normal range in later evaluations. At 18 days of life, the patient presented with high LH (24.8 IU/L, ref 0.4-7.6), while testosterone (433 ng/dL, ref 20-300) and FSH (3.1 IU/L, ref 0.3-4.1) and AMH (338 pmol/L, ref 242-1583) were within the male range. Partial androgen insensitivity was suspected, and male sex was assigned. The patient underwent hypospadias repair and received testosterone therapy to promote penile growth. At 12 years of age, the patient had no clinical signs of puberty, with a testicular volume of 3 mL bilaterally. LH, ACTH, progesterone and 17OHP were high, cortisol, androstenedione and testosterone were within the reference range for a prepubertal boy but relatively low for the elevated LH and ACTH levels (Table 1). The diagnosis was reassessed. Testosterone response to hCG (6 x 1,500 IU) was borderline, and an absent response of cortisol to the ACTH test was observed. Altogether, these observations were suggestive of impaired CYP17A1 and CYP21A2 activities. Bone X-ray imaging was normal, with no indications of Antley-Bixler syndrome (Table 2). The patient required sex steroid and corticosteroid replacement therapy.

Patient 2's sister was evaluated at 12.5 years of age with breast Tanner stage 2. Blood pressure was normal. She presented with elevated basal ACTH (297 pg/mL, ref 10-46), 17OHP (16.7 ng/mL, ref 0.6-1.7), and progesterone (33.7 ng/mL, ref 0.4-1.1). Basal cortisol was within the reference values for age (11.7 µg/dl, ref 6-21). Estradiol was low (14 pg/mL, ref 20-77), with normal LH (4.7 IU/L, ref 0.1-5.3) and high FSH (8.7 IU/L, ref 1.1-7.3). Due to the lack of pubertal progression, sex steroid hormone replacement therapy was initiated.

Patient 3 was born from reportedly nonconsanguineous parents of Argentine origin, at 39 weeks with appropriate weight and height for gestational age. The patient was raised as female and referred to us at the age of 9 years. She had previously undergone urogenital sinus correction. The patient was prepubertal (Tanner staging B1, PH1), with a clitoris measuring less than 1 cm in length and a palpable left inguinal mass, consistent with a gonad. Additionally, she presented with arachnodactyly, thoracic kyphosis, unilateral kidney agenesis, and dysmorphic features, including a bulbous nose and a flat nasal bridge. Karyotype was 46,XY. No Müllerian ducts were detected on ultrasonography. Serum AMH (162 pmol/L) was elevated for female reference (5-55 pmol/L) but low for male reference (300-1800 pmol/L), indicating the existence of testicular tissue. Basal ACTH, progesterone and 17OHP were high, whereas cortisol was low. Like in Patients 1 and 2, cortisol showed no response to the ACTH test (Table 1), suggesting impaired CYP17A1 and CYP21A2 function. Bilateral gonadectomy was performed, confirming the existence of testicular tissue without dysgenesis and supporting a steroid synthesis disorder. She required replacement therapy with hydrocortisone and sex steroids.

Patient 4 was delivered at 39 weeks with weight and height appropriate for gestational age and was referred at 5 days of life for ambiguous genitalia. The patient was the first child of reportedly non-consanguineous parents of mixed Argentine-European origin, and there was no significant family history. EGS was 4.5/12, with a phallus measuring 1 cm long and 0.3 cm wide, perineoscrotal hypospadias, partially fused labioscrotal folds, and bilateral inguinal gonads. Additionally, the patient had a bulbous nose and left preauricular skin tags. No skeletal features of Antley-Bixler syndrome were observed. Blood pressure was normal. Karyotype was 46,XY. No Müllerian ducts were observed on ultrasonography. At 19 days of life, testosterone was low (23 ng/dl, ref 20-300), with elevated LH (12.9 IU/L, ref 0.4-7.6) and normal AMH level (696 pmol/L, ref 242-1583) and FSH (3.8 IU/L, ref 0.3-4.1), suggesting a 46,XY DSD due to a disorder of androgen synthesis. Male sex was assigned. At 8 months of life, testosterone secretion in response to hCG (6 x 1500 IU) was insufficient (Table 1). Basal ACTH, progesterone and 17OHP were high; basal cortisol was within the reference range but showed no changes after ACTH stimulation. An impaired CYP17A1 and CYP21A2 activity was suspected. The patient presented an adequate increase in penile size after testosterone administration. Surgical correction of hypospadias and bilateral orchidopexy were performed. A

 doi:10.20944/preprints202510.0422.v1

critical observation from this case series is the variable expressivity of the Antley-Bixler Syndrome (ABS) skeletal phenotype. Despite sharing an identical homozygous G88S genotype, only Patient 3 presented with dysmorphic features consistent with ABS, whereas the other four individuals did not have significant skeletal malformations (Table 2).

The POR G88S mutation is present in multiple unrelated Argentine families. Targeted exome NGS in patient 1 showed an average coverage of 72x, with ≥20× coverage in 92% of bases in the virtual gene panel. The initial analysis identified 27952 variants in 4496 genes. Filtering for read depth ≥10x and GQ score ≥45, yielded 2040 variants in 1014 genes. Further analysis considering 21 candidate genes for 46,XY DSD available in the TruSight One sequencing panel and MAF <1% in available population databases revealed only one relevant variant in exon 4 of POR gene: NM_001395413.1:c.253G>A; NP_001382342.1:p.Gly88Ser. The position was read with a depth of 41X, with the adenine at position 253 in 41 reads, compatible with a homozygous presentation. The variant was confirmed by Sanger sequencing in the patient and segregation analysis indicated that his mother was heterozygous for the same variant. Paternal DNA was not available (Figure 2). The same homozygous variant was found in patients 2, 3 and 4 by Sanger sequencing, although a hemizygous presentation with a paternal allele deletion cannot be completely ruled out in cases 1 and 3. The sister of patient 2 carried the same homozygous variant in the POR gene while both parents were heterozygous. Patient 3's mother had the same variant in heterozygous state, and paternal DNA was not available. Both parents of patient 4 were heterozygous for the same variant. The pedigrees show the inheritance pattern of the mutation, with the index cases (affected individuals) marked by arrows. The pedigrees also indicate the genotypes of the family members, with full black symbols representing individuals with the POR deficiency phenotype and full white symbols representing those without the phenotype. The G88S and WT alleles are denoted by specific symbols.

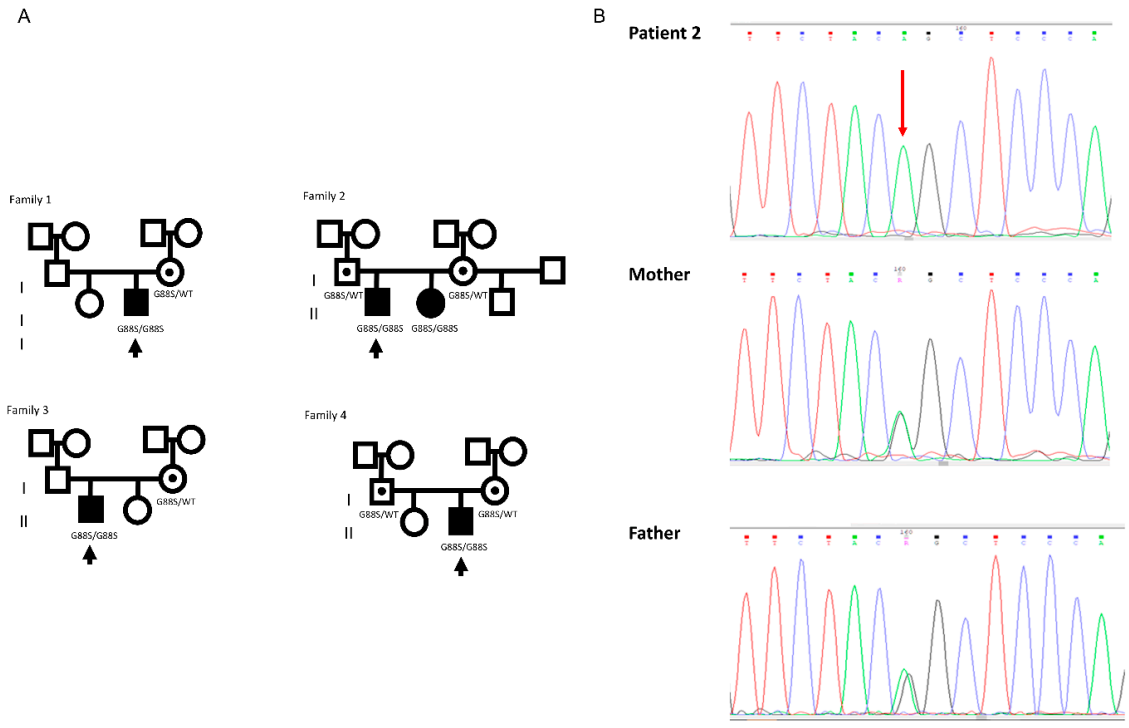

Figure 2. Pedigrees of four unrelated Argentine families with POR deficiency due to the G88S mutation. A. The family trees of four distinct families (Family 1, Family 2, Family 3, and Family 4) from Argentina, in which at least one individual was diagnosed with POR deficiency and found to be homozygous for the G88S mutation in the *POR* gene. In each pedigree, squares represent males, and circles represent females. Filled symbols indicate individuals affected by POR deficiency. The inheritance pattern observed in these families is consistent with autosomal recessive inheritance. **B. Sanger sequencing analysis confirming the homozygous G88S mutation in Patient 2 and heterozygous carrier status in the parents.** The top panel shows the chromatogram for Patient

 doi:10.20944/preprints202510.0422.v1

2, revealing a homozygous guanine to adenine (G>A) transition at nucleotide position c.262 (indicated by the arrow). This mutation results in the substitution of glycine (Gly) to serine (Ser) at amino acid position 88 (p.Gly88Ser or G88S) in the POR protein. The middle and bottom panels show the chromatograms for the mother and father.

The G88S variant was present in gnomAD exomes v4.1 (A=0.0000143; 21/1613454) with rs782213151 (dbSNP v.157) and absent in gnomAD genomes and in our own in-house database including over 800 Argentine individuals. After considering in vitro functional studies performed here, showing variant characterization (see below), the variant was classified as Pathogenic (10 points) since it met the following ACMG/AMP criteria: PM1 (moderate, 2 points), PM2 (supporting, 1 point), PM3 (supporting, 1 point), PP3 (moderate, 2 points), PS3 (strong, 4 points).

Glycine 88 Is Located near FMN Binding Site in POR and Mutation G88S Creates Protein Instability

Human POR has distinct domains for the binding of NADPH/FAD and FMN. The FMN binding domain interacts with the redox partners and is required for electron transfer to partner proteins [94,95]. The redox equivalents for the electron transfer are provided by NADPH which is used as a substrate by POR and converted to NADP. The G88S mutation causes the replacement of the amino acid glycine (G) with serine (S) at the 88th position of the POR protein. This substitution occurs within the critical FMN binding domain of the POR protein. The functional importance of the Glycine residue at position 88 (G88) in human POR is underscored by its high degree of conservation across a wide range of species (Figure 3A). This conservation, spanning from mammals to insects, suggests that this amino acid plays a critical role in the structure or function of the POR protein.

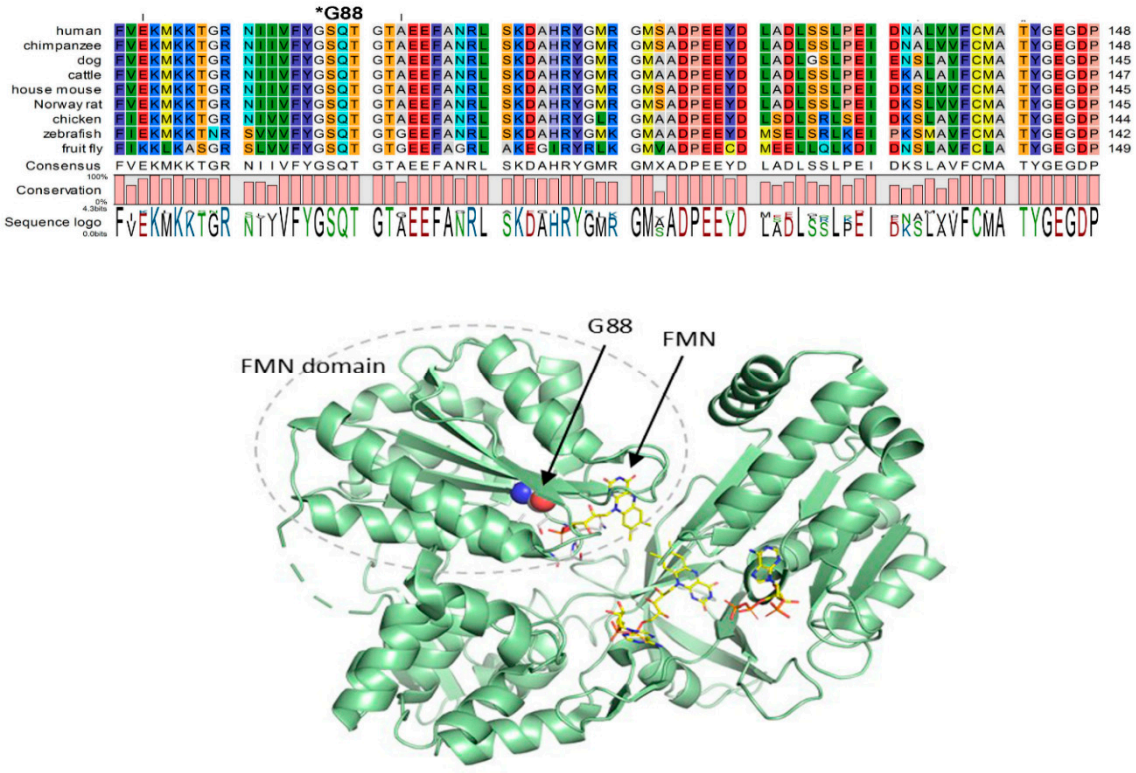

Figure 3. Sequence conservation and location of G88 residue in POR. A. Conservation of Glycine 88 (G88) in P450 oxidoreductase (POR) across different species. A multiple sequence alignment of a conserved region of the POR protein from various species, including human, chimpanzee, dog, cattle, house mouse, Norway rat, chicken, zebrafish, and fruit fly. The alignment shows a high degree of conservation of glycine 88 residue across evolutionarily diverse species. **B. A structural model of the human POR protein.** The location of the Glycine 88 residue, which is substituted by Serine in the G88S mutation, is indicated. The G88S mutation site is located in

 doi:10.20944/preprints202510.0422.v1

close proximity to the FMN binding domain of POR. This spatial relationship suggests that the G88S substitution may affect the binding and stability of the FMN cofactor, potentially disrupting the electron transfer function of POR.

To obtain a more comprehensive understanding of how the G88S mutation may affect the protein's structure and function, we have analysed the interactions between the protein and the cofactor FMN in the human wild-type POR (POR-WT) and in models of the mutant POR (POR-G88S). In the experimentally determined structure of human POR the cofactor FMN is bound to the protein by both hydrophobic and polar interactions (Figure 4). The isoalloxazine ring in sandwiched between Tyr143 and Tyr181 maximizing favourable p-p interactions, whereas the phosphate group is situated in a shallow cavity formed by residues in the loop between b-strand 1 and a-helix B (nomenclature according to Wang 1992). In this loop, the S89 and T91 side-chain oxygen atoms and the Q90, T91 and T93 backbone nitrogen atoms are all making hydrogen bonds to the terminal oxygen atoms in the phosphate group.

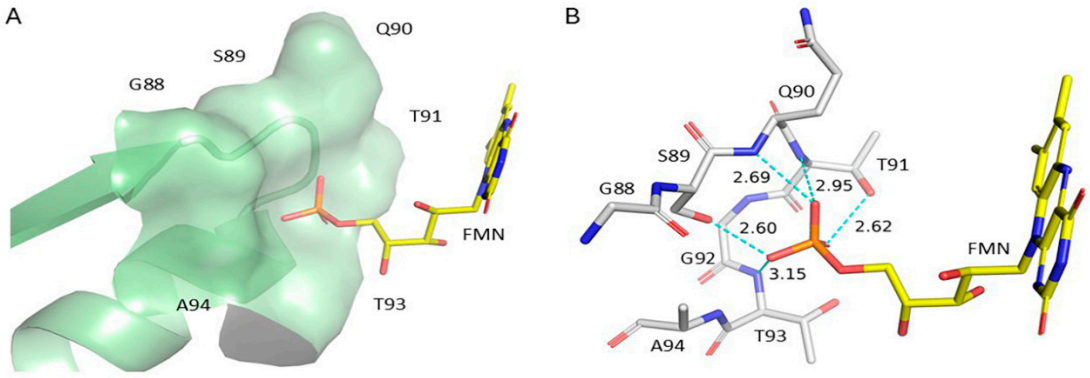

Figure 4. Interactions between POR-WT and the FMN Cofactor. (A) Structural representation highlighting the loop region (residues 88-94, depicted with surface) between β-strand 1 and α-helix B in wild-type human POR (PDB: 3QE2). This loop forms a cavity crucial for positioning the phosphate group of the FMN cofactor (shown in stick representation). Key residues within this loop (G88, S89, Q90, T91, G92, T93, A94) contribute to FMN binding. **(B) Detailed view of the hydrogen bonding network stabilizing the FMN phosphate group within the binding cavity.** Specific hydrogen bonds (dashed lines) are shown between the phosphate oxygen atoms and the side-chain oxygen atoms of Serine 89 (S89) and Threonine 91 (T91), as well as the backbone nitrogen atoms of Glutamine 90 (Q90), Threonine 91 (T91), Glycine 92 (G92) and Threonine 93 (T93). Distances are indicated in Angstroms (Å). These interactions anchor the FMN cofactor in its functional position within the WT enzyme.

Comparison of the POR-WT structure and POR-G88S model reveals that there is no direct contact between the residue in position 88, G88 or S88, respectively, and FMN. Mutation may often have an indirect effect, and we speculated on the effect of the glycine 88, being located at the end of a strand influenced the conformation of the subsequent loop comprising residues 88-94 which was altered due to G88S mutation (Figure 5). We therefore performed molecular dynamics (MD) simulations on the POR-WT and POR-G88S structures and looked for differences caused by the mutation (Figure 6). MD simulation of POR-WT showed that binding of FMN and the hydrogen-bonding pattern between the protein and FMN after an initial minor rearrangement remained stable during the simulation. The corresponding MD simulation of POR-G88S showed a nearly identical behaviour with an initial minor rearrangement of the intramolecular hydrogen bonds followed by a stable system. Both MD simulations were characterised with smaller fluctuations for the hydrogen bonds involving the hydroxy sidechains of S89 and T91 compared to the fluctuations of the hydrogen bonds involving the backbone nitrogen atoms. To identify, if the mutation imposes an effect on the

 doi:10.20944/preprints202510.0422.v1

conformation of the loop, we compared the phi and psi angles of the residues 88-90 in POR-WT and POR-G88S (Figure 7). The G88S mutation influences the backbone conformation of the loop with the position 88 Psi dihedral angle increasing by more than 40° and the remaining dihedral changed by roughly 10°. Although this may not represent major changes, it may contribute to a weakening of the binding of FMN.

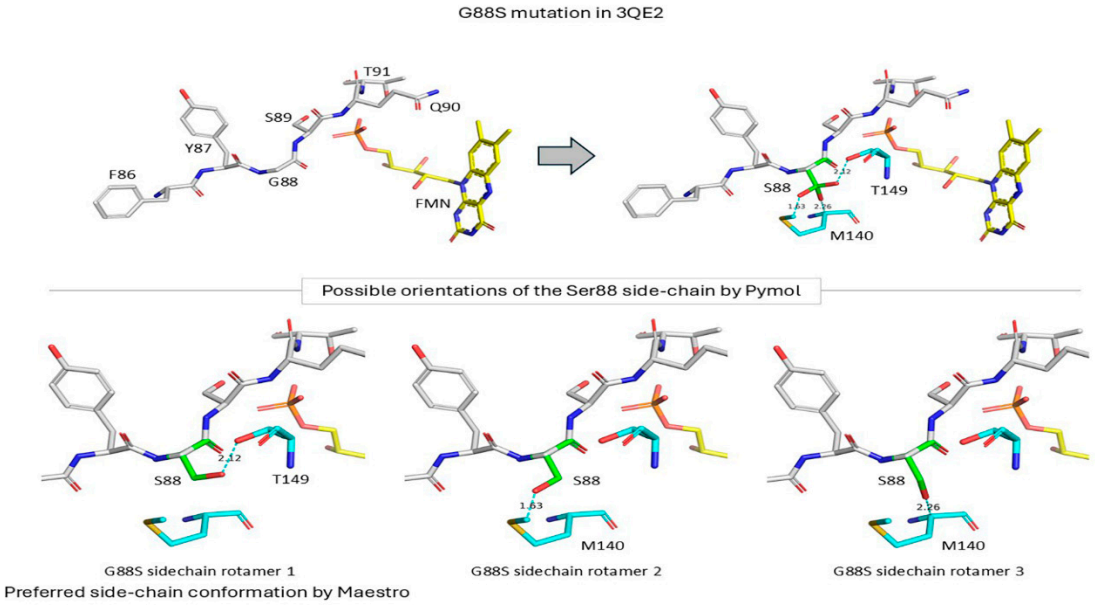

Figure 5. In Silico Mutagenesis Modeling the G88S Substitution in Human POR. Structural comparison showing the local environment around residue 88 in the wild-type POR structure (PDB: 3QE2, left panel) and the modeled G88S mutant (right panel). The WT Glycine 88 (G88) is shown interacting with neighboring residues (F86, Y87, S89, Q90, T91) and the FMN cofactor. The right panel depicts the substitution with Serine (S88), illustrating potential steric or electronic changes introduced by the larger, polar side chain. Below, possible side-chain rotamers (conformations) for the introduced Serine 88 residue are shown as predicted by PyMol (top row) and Maestro (bottom row), highlighting the conformational flexibility and potential new interactions or clashes introduced by the mutation near the FMN binding site.

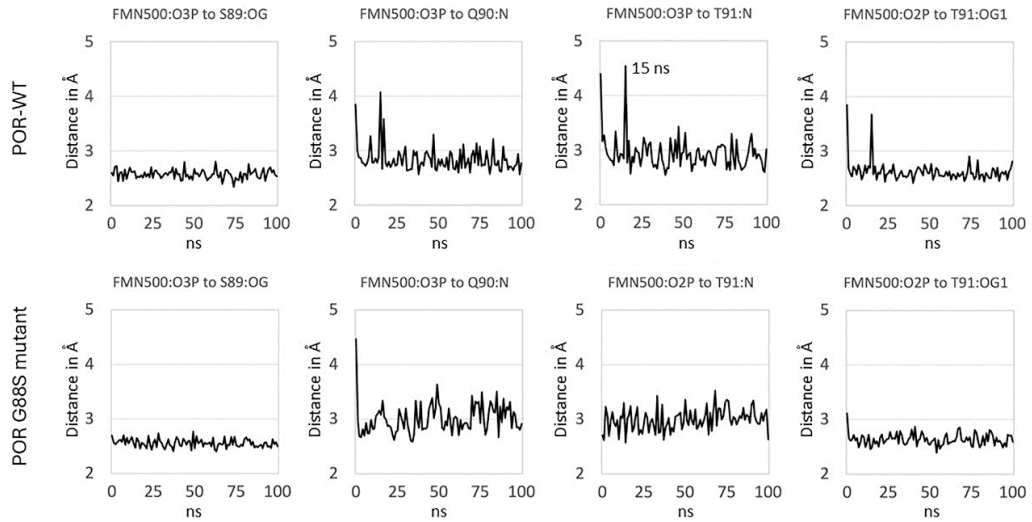

 doi:10.20944/preprints202510.0422.v1

Figure 6. Stability of FMN Interactions During Molecular Dynamics (MD) Simulations. Plots showing key distances (in Å) between specific FMN phosphate oxygen atoms (O2P, O3P) and interacting protein residues (S89 side chain oxygen–OG, Q90 backbone nitrogen–N, T91 backbone nitrogen–N, T91 side chain oxygen–OG1) over the course of a 100 ns MD simulation. The upper row represents the simulation for POR-WT, showing relatively stable distances and hydrogen bonding patterns after initial equilibration. The lower row represents the simulation for the POR-G88S mutant, also showing relative stability in these specific interactions during the simulation, suggesting the closed conformation might retain FMN binding, although potentially weakened as suggested by dihedral angle changes (Figure 7) and overall protein instability causing significant loss of flavins (Figure 9). Note the transient increase in distance around 15 ns for the FMN:O3P to T91:N interaction in the WT simulation.

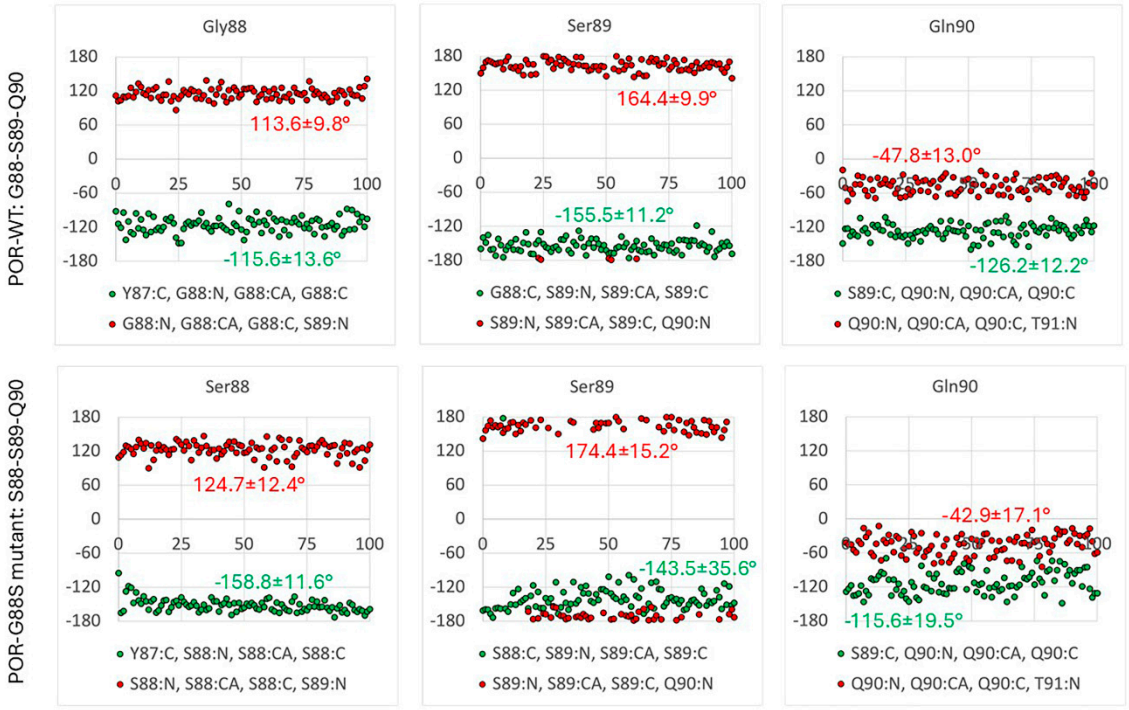

Figure 7. Backbone Torsional Angle Variations in the FMN Binding Loop During MD Simulations. Torsional angles of the ^{88}GSQ^{90} loop in POR WT (upper row) and the corresponding ^{88}SSQ^{90} loop in the POR G88S mutant (lower row). Analysis comparing the phi (Φ, Cα-N bond rotation) and psi (Ψ, Cα-C bond rotation) backbone dihedral angles for residues 88, 89, and 90 in POR-WT (upper row) versus the POR-G88S mutant (lower row) over the 100 ns MD simulation is shown. Red dots represent Ψ angles, green dots represent Φ angles. Median values ± standard deviations are indicated. The G88S mutation causes notable shifts, particularly an increase of >40° in the Ψ angle of residue 88 (comparing G88 Ψ ~ -115.6° in WT vs S88 Ψ ~ -158.8° in mutant) and smaller (~10-20°) changes in other angles within the 88-SSQ-90 loop. These conformational alterations, although seemingly minor, may contribute to weakening FMN binding or altering loop dynamics, potentially affecting protein stability or function.

The effect of the G88S mutation may not necessary be associated with a reduced flavin binding in the closed form of POR but could also be an upstream effect on the open form. The models for the open form of POR were based on the FMN domain extracted from the 3D structure of the open form of rat POR (PDB 3ES9) and the G85S mutant (corresponding to the G88S mutant in human POR). MD simulations of these two models showed that the FMN domain of the rat POR WT was stable for the 500 ns simulation and that FMN, after a minor initial rearrangement, remained in the binding site as determined by X-ray crystallography (Figure 8A-C). The corresponding MD simulation of the rat POR G85S mutant showed that the protein made a conformational change after 250 ns, that the ligand

 doi:10.20944/preprints202510.0422.v1

subsequently changed its position relative to the protein after 400 ns and that several distinct conformational changes could be identified (Figure 8D-F).

Based on the understanding of POR and the potential impact of mutations, the G88S mutation may affect POR in multiple ways. Altered FMN Binding: The G88S mutation is located within the FMN-binding domain [96]. This mutation may disrupt the binding of FMN to POR, potentially affecting electron transfer. This disruption could occur due to changes in the shape of the binding site or alterations in the electrostatic interactions between FMN and POR. Although the G88 residue is located within the FMN binding region, the impact on both flavin cofactors (Figure 9) suggests a broader consequence of the mutation on protein stability. Reduced POR Activity: Impaired FMN binding or other structural changes caused by the mutation could reduce the overall activity of POR. This reduction in activity could result from a decrease in the efficiency of electron transfer or a disruption in the interaction between POR and its partner P450 enzymes. Disrupted Interactions with P450 Enzymes: The mutation may affect the interaction between POR and its partner P450 enzymes, leading to reduced P450 activity. This disruption could be due to changes in the binding interface between POR and P450 enzymes or alterations in the conformational dynamics of the POR-P450 complex.

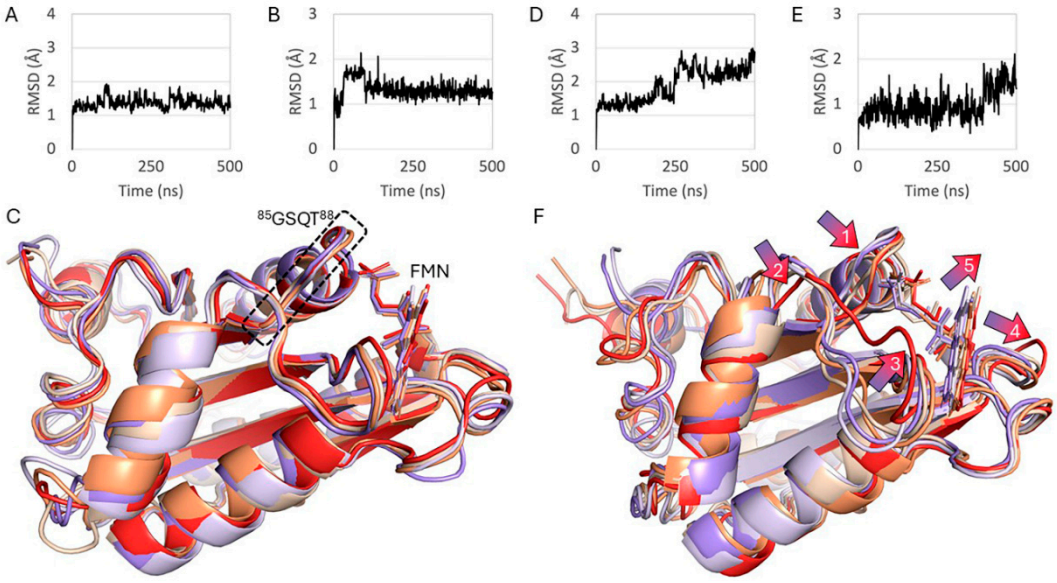

Figure 8. MD simulations of FMN domain in 3NS9 WT and 3NS9 G85S mutant (equivalent to human G88S). A-C) Data for rat 3NS9 WT. D-F) Data for rat 3NS9 G85S mutant. A and D) RMSD for protein Ca atoms. B and E) RMSD for ligand relative to protein. C and F) Overlap of structures after 100 (blue), 200 (cyan), 300 (beige), 400 (brown) and 500 (red) ns MD simulation. F) Arrows indicating the conformational changes relative to the initial structure: i) ^{85}GSQT^{88} loop moved towards FMN arrow 1), ii) ^{140}GEGDPTDNA^{149} sequence underwent drastic conformational change (arrow 2 and 3), iii) ^{209}DG^{210} loop moved away from FMN (arrow 4), and iv) FMN shifted slightly out of the originally defined binding pocket (arrow 5).

POR mutations can be categorized based on their location and their impact on POR protein function. These mutations can be broadly classified into those that disrupt the FAD-binding domain, those that affect the FMN-binding domain, and those that impact the interaction surface between POR and P450 enzymes [1]. Each of these mutation types can lead to distinct functional consequences for the POR protein and associated P450 enzyme activities. The FMN-binding domain, where the G88S mutation is located, is crucial for POR's role as an electron carrier [97]. POR utilizes FMN to transfer electrons from NADPH to P450 enzymes, enabling them to carry out their diverse catalytic functions. Disruptions in the FMN-binding domain, such as those caused by the G88S mutation, can

 doi:10.20944/preprints202510.0422.v1

impair POR's electron transfer capabilities, leading to reduced P450 enzyme activity and potential downstream effects on steroidogenesis and drug metabolism.

To validate these predictions, we carried out a number of experiments to elucidate the specific functional impact of the G88S mutation on POR protein structure, electron transfer kinetics, and P450 enzyme interactions.

The G88S mutation in POR leads to a significant reduction in both FMN and FAD content. To investigate the impact of the G88S mutation on the flavin cofactor binding of POR, we measured the FMN and FAD content of purified recombinant WT and G88S POR proteins. The G88S variant exhibited a marked decrease in both flavin cofactors. The FMN content in the G88S mutant was reduced to approximately 30% of the wild-type level (Figure 9A). Notably, the FAD content was even more severely affected, with the G88S mutant retaining only about 15% of the FAD levels observed in the WT protein (Figure 9B). These reductions in flavin content were statistically significant ($p < 0.05$ for FMN and $p < 0.001$ for FAD).

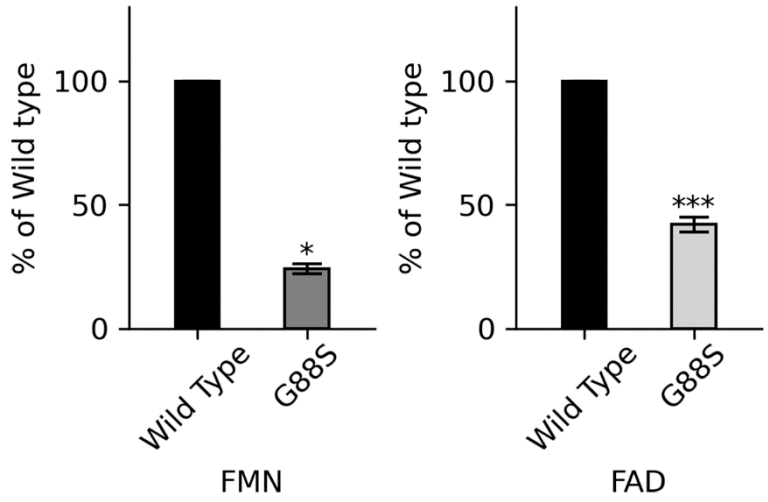

Figure 9. Flavin mononucleotide (FMN) and flavin adenine dinucleotide (FAD) content of wild-type (WT) and G88S mutant POR. Flavin content was determined by measuring the fluorescence of released FMN and FAD from purified WT and G88S POR proteins. The electron transfer from POR to its redox partners is mediated by its two obligatorily bound flavin cofactors, FAD and FMN. The G88S mutation in POR leads to a significant reduction in both FMN and FAD content, suggesting a potential mechanism for the impaired activity observed in individuals with this mutation. (**A) Bar graph showing the relative FMN content in G88S POR compared to WT POR. (B) Bar graph showing the relative FAD content in G88S POR compared to WT POR.** Statistical significance was determined by Student's t-test to analyze the differences within experimental subsets, with *$p < 0.05$ and ***$p < 0.001$. Data are presented as mean ± standard deviation from at least three independent experiments.

While the direct impact of the mutation would likely be on the binding of FMN, the substantial reduction in FAD levels suggests a broader effect on protein stability and/or cofactor binding. One plausible explanation is that the G88S substitution alters the FMN binding domain, which may consequently affect the overall folding and stability of the protein. Such instability could lead to a decreased ability to retain both FMN and FAD, potentially through increased cofactor dissociation or protein degradation. The more pronounced reduction in FAD levels might indicate that the structural perturbation caused by the G88S mutation has a more destabilizing effect on the FAD binding environment, possibly through allosteric mechanisms or by affecting the interactions between the FMN and FAD binding domains within the POR molecule.

The G88S mutation in POR severely impairs its NADPH-dependent reductase activity towards various small molecule substrates. The G88S mutation's impact on POR activity was evaluated by expressing both wild-type (WT) and mutant POR-G88S in E. coli as N-23 forms and purifying

 doi:10.20944/preprints202510.0422.v1

bacterial membranes. The capacity of POR-WT and POR-G88S to transfer electrons from NADPH to cytochrome c, MTT, and resazurin was assessed. As depicted in Figure 10A, the G88S POR variant exhibited a significantly decreased ability to reduce cytochrome *c* compared to the WT enzyme across a range of substrate concentrations.

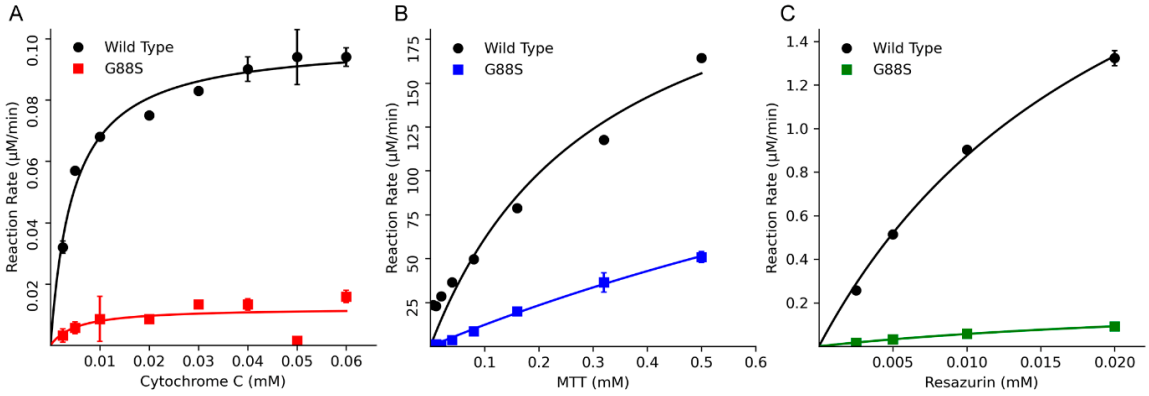

Figure 10. Kinetic analysis of small molecule reduction by wild-type (WT) and G88S POR. The NADPH-dependent reductase activity of purified WT and G88S POR was assessed using three different electron acceptor substrates. The reaction rates were measured at varying substrate concentrations and the data were fitted to the Michaelis-Menten equation to determine the kinetic parameters. **(A) Cytochrome *c* reduction assay.** The rate of cytochrome *c* reduction was monitored spectrophotometrically at 550 nm. The WT POR exhibited typical Michaelis-Menten kinetics, whereas the G88S variant showed a significantly reduced maximal velocity (Vmax) and potentially altered substrate affinity (Km). **(B) 3-(4,5-dimethylthiazol-2-yl)-2,5-diphenyltetrazolium bromide (MTT) reduction assay.** The reduction of MTT to formazan was measured spectrophotometrically at 570 nm. Similar to cytochrome *c* reduction, the G88S POR displayed a markedly lower reductase activity compared to the WT enzyme across a range of MTT concentrations. **(C) Resazurin reduction assay.** The reduction of the non-fluorescent resazurin to the fluorescent resorufin was monitored by measuring fluorescence (excitation at 560 nm, emission at 590 nm). The G88S POR showed a severely impaired ability to reduce resazurin compared to the WT POR, indicating a significant defect in its electron transfer capability to this substrate. These results demonstrate that the G88S mutation in POR leads to a substantial decrease in its reductase activity towards various electron acceptors.

Kinetic analysis revealed a marked decrease in the catalytic efficiency (Vmax/Km) of the G88S mutant for cytochrome *c*, which was only 2.93% of the WT activity (Table 3). Similarly, the reduction of MTT (Figure 10B) was also substantially impaired in the G88S variant, showing a catalytic efficiency of only 26% of the WT (Table 3). The most dramatic effect was observed in the resazurin reduction assay (Figure 10C), where the G88S POR displayed a severely compromised activity, with a catalytic efficiency of only 8% of the WT (Table 3). These results collectively demonstrate a deleterious defect in the electron transfer capability of the G88S POR mutant.

Table 3. Kinetic parameters of wild-type (WT) and G88S POR for different substrates. The table summarizes the kinetic parameters obtained for recombinant WT and G88S POR expressed in bacteria using cytochrome *c*, MTT, and resazurin as substrates.

	Vmax (nmol/min/ mmol of POR)	Km (μM)	Vmax/Km (% of WT)
Cytochrome c reduction activity			
WT	78.1	4.6	16.9 (100)
G88S	19.9	39.5	0.5 (2.93)

 doi:10.20944/preprints202510.0422.v1

MTT reduction activity			
WT	44.8	138.4	0.32 (100)
G88S	68	805	0.08 (26)
Resazurin reduction activity			
WT	2197	22	101 (100)
G88S	207	27	8 (8)

The significant reduction in the reductase activity of the G88S POR mutant towards multiple small molecule substrates (cytochrome *c*, MTT, and resazurin) is consistent with the observed loss of flavin cofactors (Figure 10) and likely contributes to the overall POR deficiency associated with this mutation. As the G88S mutation is located in the FMN binding domain, the observed protein instability, as suggested by the reduced flavin content, could directly impact the efficiency of electron transfer from NADPH through FAD and FMN to downstream acceptors.

Steroid metabolizing enzyme Activity–After observing decreased activity of the G88S POR mutant in reducing small molecule substrates, we investigated the impact of this mutation on the activity of key steroid-metabolizing cytochrome P450 enzymes, which rely on POR for their enzymatic function. To determine the functional consequences of the G88S mutation in POR on steroid hormone biosynthesis, we assessed the ability of the mutant protein to support the activities of CYP17A1 and CYP21A2, two crucial enzymes in the steroidogenic pathway. The G88S POR variant exhibited a dramatic reduction in its capacity to support the 17α-hydroxylase activity of CYP17A1, with the observed activity being only 7% of that supported by WT POR (Figure 11A). Similarly, the 17,20-lyase activity of CYP17A1 was also severely affected, with the G88S POR supporting only 5.5% of the WT activity (Figure 11B). The impact of the G88S mutation was even more pronounced on the 21-hydroxylase activity of CYP21A2, where the mutant POR supported a mere 1.3% of the activity observed with WT POR (Figure 11C). These results indicate a major impairment in the ability of the G88S POR variant to transfer electrons to these key steroidogenic enzymes. These in vitro findings provide a direct molecular explanation for the patients' clinical biochemistry (Table 1). The devastating >98% loss of CYP21A2 activity correlates perfectly with the observed CAH-like phenotype, while the >94% loss of CYP17A1 17,20-lyase activity explains the impaired androgen and estrogen synthesis central to the patients' gonadal dysfunction (Table 4).

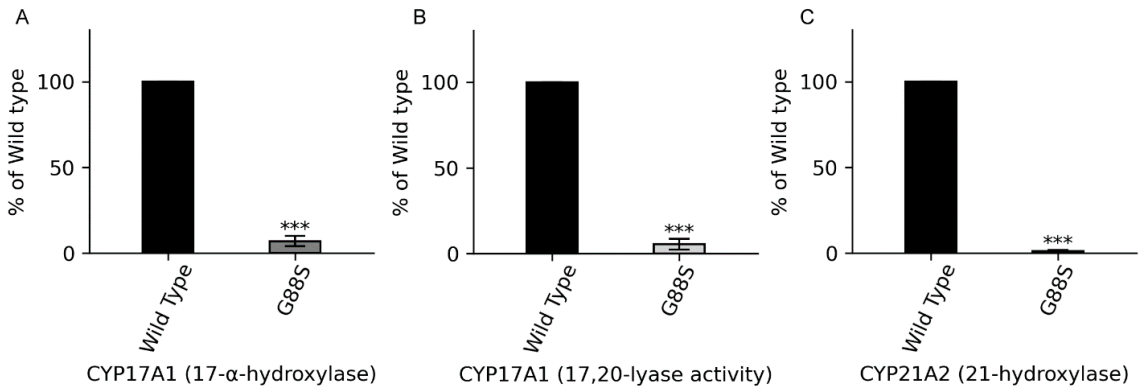

Figure 11. CYP17A1 and CYP21A2 activities supported by wild-type (WT) and G88S POR. The ability of WT and G88S POR to support the activities of two key steroidogenic cytochrome P450 enzymes, CYP17A1 and CYP21A2, was assessed in vitro. (A) CYP17A1 17-α-hydroxylase activity, which catalyzes the conversion of pregnenolone to 17-hydroxypregnenolone and progesterone to 17-hydroxyprogesterone, is severely impaired when supported by G88S POR, showing only 7% of the WT activity. (B) CYP17A1 17,20-lyase activity, which further converts 17-hydroxypregnenolone to dehydroepiandrosterone (DHEA), essential for the production of adrenal androgens, is also significantly reduced with G88S POR, exhibiting only 5.5% of the WT activity. (C)

 doi:10.20944/preprints202510.0422.v1

CYP21A2 21-hydroxylase activity, which is responsible for the conversion of 17-hydroxyprogesterone to 11-deoxycortisol (a precursor of cortisol) and progesterone to 11-deoxycorticosterone (a precursor of aldosterone), is most severely affected by the G88S mutation in POR, with the mutant supporting only 1.3% of the WT activity. Loss of CYP21A2 activity leads to congenital adrenal hyperplasia (CAH), characterized by impaired cortisol and aldosterone synthesis and an overproduction of androgens. Statistical significance was determined by Student's t-test to analyze the differences within experimental subsets, with ***$p < 0.001$ compared to WT in all assays. Data are presented as mean ± standard deviation from at least three independent experiments.

Table 4. In Vitro Functional Data for WT and G88S POR. A consolidated summary of the in vitro enzymatic activities of wild-type (WT) and G88S mutant P450 oxidoreductase (POR), presented as a percentage of the WT activity.

Enzyme / Activity	WT Activity (% of WT)	G88S Activity (% of WT)
Flavin Cofactor Content		
FMN Content	100%	<30%
FAD Content	100%	<15%
Small Molecule Reduction		
Cytochrome c Reduction	100%	2.93% (catalytic efficiency)
MTT Reduction	100%	26% (catalytic efficiency)
Resazurin Reduction	100%	8% (catalytic efficiency)
Steroidogenic CYP Activities		
CYP17A1 (17α-hydroxylase)	100%	7%
CYP17A1 (17,20-lyase)	100%	5.5%
CYP21A2 (21-hydroxylase)	100%	1.3%
Drug-Metabolizing CYP Activities		
CYP3A4	100%	3.3%
CYP3A5	100%	9%
CYP2C9	100%	3%
CYP2C19	100%	4%

The G88S mutation in POR leads to a substantial reduction in the activities of major drug-metabolizing cytochrome P450 enzymes. To investigate the impact of the G88S POR variant on drug metabolism, we assessed its ability to support the activities of several key human cytochrome P450 enzymes: CYP3A4, CYP3A5, CYP2C9, and CYP2C19. The CYP3A4 activity supported by the G88S variant was reduced to 3.3% of the WT level (Figure 12A). CYP3A5 activity was also significantly impaired, with the G88S POR supporting only 9% of the WT activity (Figure 12B). Similarly, the activities of both CYP2C9 and CYP2C19 were severely compromised, showing only 3% (Figure 12C) and 4% (Figure 12D) of the respective WT activities when supported by the G88S POR. These findings demonstrate a broad and significant impairment in the ability of the G88S POR mutant to facilitate

 doi:10.20944/preprints202510.0422.v1

the catalytic functions of major drug-metabolizing enzymes. The severe reduction in the activities of CYP3A4, CYP3A5, CYP2C9, and CYP2C19 observed with the G88S POR variant has significant implications for drug metabolism in individuals carrying this mutation. These four enzymes are responsible for the biotransformation of a vast array of clinically important drugs, collectively accounting for the metabolism of a large proportion of prescribed medications.

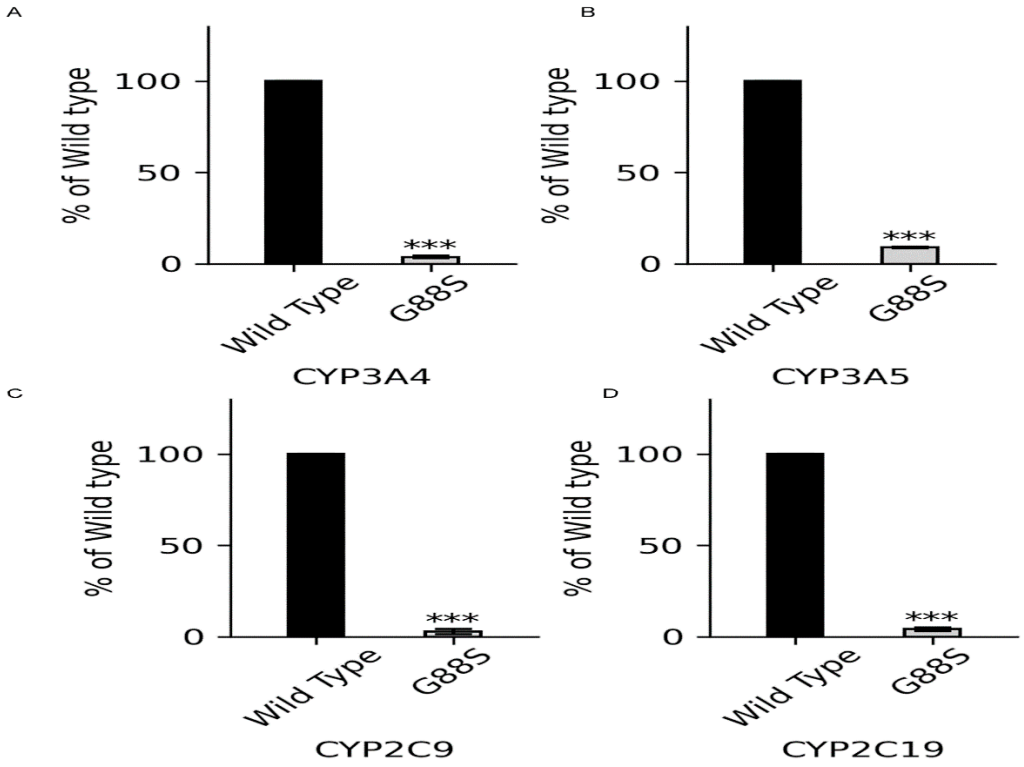

Figure 12. Activities of major drug-metabolizing cytochrome P450 enzymes supported by wild-type (WT) and G88S POR. (A) CYP3A4, the most abundant drug-metabolizing enzyme in the liver, is responsible for the metabolism of approximately 50% of clinically used drugs, including statins (e.g., atorvastatin, simvastatin), calcium channel blockers (e.g., amlodipine, nifedipine), immunosuppressants (e.g., cyclosporine, tacrolimus), and many others. The G88S POR variant supports only 3.3% of the WT CYP3A4 activity, indicating a severe impairment in the metabolism of numerous medications. (B) CYP3A5 from the CYP3A subfamily with overlapping substrate specificity to CYP3A4, is more variable among individuals. The G88S POR variant supports 9% of the WT CYP3A5 activity, suggesting a significant reduction in its function. (C) CYP2C9 is a major CYP2C subfamily enzyme involved in the metabolism of around 15% of clinically used drugs, including nonsteroidal anti-inflammatory drugs (NSAIDs) like ibuprofen and naproxen, the anticoagulant warfarin, and oral hypoglycemic agents like glipizide. The G88S POR variant supports only 3% of the WT CYP2C9 activity, indicating a substantial impact on the metabolism of these commonly prescribed medications. (D) CYP2C19 is another key enzyme in the CYP2C subfamily involved in the metabolism of several important drugs, including proton pump inhibitors (PPIs) like omeprazole and lansoprazole, antiplatelet agents like clopidogrel, and some antidepressants and antiepileptics. The G88S POR variant supports only 4% of the WT CYP2C19 activity, highlighting a significant reduction in its capacity to metabolize these drugs. The severely compromised ability of the G88S POR variant to support the activities of these major drug-metabolizing enzymes underscores the potential for altered drug pharmacokinetics, including reduced drug clearance and increased risk of adverse drug reactions, in individuals carrying this mutation. Statistical significance was determined by Student's t-test to analyze the differences within experimental subsets, with ***$p < 0.001$ compared to WT in all assays. Data are presented as mean ± standard deviation from at least three independent experiments.

 doi:10.20944/preprints202510.0422.v1

Discussion

The G88S mutation in POR, identified in four unrelated Argentine families, is a missense mutation resulting in the substitution of glycine for serine at position 88. The clinical presentations of the five patients from four unrelated families homozygous for the G88S mutation reveal a crucial nuance in the understanding of PORD, demonstrating a textbook example of variable expressivity. While all affected individuals show the biochemical and genital abnormalities characteristic of severe PORD, a striking finding is the variable presence of skeletal malformations associated with Antley-Bixler Syndrome (ABS) [2–4,8,98]. Patient 3 presents with classic dysmorphic and skeletal features of ABS, including arachnodactyly, thoracic kyphosis, and a bulbous nose. In contrast, the other three 46,XY male patients, who share the identical G88S homozygous genotype, have no significant skeletal features of ABS. This proves that the G88S mutation, while causing a severe biochemical defect, is not sufficient to produce the full ABS skeletal phenotype on its own. This strongly suggests the existence of other modulating factors, such as genetic or environmental modifiers or subtle epigenetic influences, that contribute to the clinical expression of the disease. A significant finding of this study is the identification of the identical homozygous p.Gly88Ser mutation in four apparently unrelated families of Argentine origin. This variant is exceedingly rare in global population databases (gnomAD allele frequency ~1.4×10−5), making its recurrence in a specific geographic cohort highly suggestive of a founder effect. While definitive proof would require haplotype analysis to demonstrate a shared chromosomal background among the affected individuals, the recurrence of this novel and severe mutation strongly suggests it may represent a regional founder allele. This has important clinical implications, suggesting that *POR* c.262G>A should be considered for targeted screening in Argentine patients presenting with disorders of sex development and/or biochemical evidence of combined CYP17A1 and CYP21A2 deficiency.

Furthermore, the case of the 46,XX patient (the sister of Patient 2) with delayed puberty, rather than the expected virilization, adds a crucial piece to the understanding of PORD's clinical spectrum. The in vitro assays demonstrated that the G88S variant severely impairs CYP17A1 17,20-lyase activity, reducing it to only 5.5% of wild-type. This enzyme is essential for gonadal androgen and estrogen production. The severity of this defect is so strong that it blocks both pathways, leading to the low estradiol levels observed in the patient and consequently, a failure of pubertal development. The elevated basal and stimulated levels of 17OHP and progesterone across all patients strongly correlate with the severely impaired CYP21A2 activity observed in vitro (Figure 10C), where the G88S POR supported only 1.3% of WT activity. This leads to a block in the cortisol synthesis pathway, as reflected by the inadequately low or normal cortisol for the elevated ACTH levels. This finding reinforces the direct link between the molecular defect and the clinical presentation, highlighting the need for a nuanced understanding of PORD beyond the classic virilization phenotype [7,31,99–103].

The high degree of evolutionary conservation of this glycine residue, spanning from mammals to insects, underscores its critical functional importance. The substitution of this small, flexible amino acid with a bulkier, polar serine likely perturbs the delicate structural integrity of the FMN-binding domain, leading to the molecular pathology observed. To elucidate the mechanism by which this localized mutation causes a widespread functional deficit, detailed structural and molecular dynamic analyses were performed. While in silico modeling of the closed POR conformation showed only minor changes in the in backbone angles, such as a greater than 40° shift in the Psi (Ψ) dihedral angle of the 88th residue, with the FMN cofactor remaining in its binding pocket, a more powerful mechanistic explanation emerges from the dynamic simulations of the open conformation [104]. Unlike mutations that may locally disrupt a static cofactor binding pocket, our simulations of the *open conformation* reveal that G88S fundamentally compromises the protein's essential dynamic flexibility. This dynamic failure propagates through the protein's structure, leading to global misfolding, an inability to properly bind *both* FMN and FAD, and subsequent degradation. This demonstrates that the mutation does not simply weaken cofactor binding in a static, stable protein, but rather fundamentally compromises the protein's dynamic flexibility, which is essential for its function. The substitution likely perturbs the protein's folding or maturation process, resulting in a large

 doi:10.20944/preprints202510.0422.v1

population of misfolded, flavin-deficient, and unstable protein that is then rapidly degraded. This is the definitive explanation for the severe loss of flavin cofactors observed experimentally (<30% FMN, <15% FAD).

To contextualize the severity of the G88S mutation, its functional profile was compared with that of other well-characterized POR mutations. A key precedent for protein instability is the L374H mutation, which affects a flexible hinge region of the POR protein and also causes a severe loss of flavin content [32]. A quantitative comparison reveals that both mutations lead to a severe loss of enzymatic activity, but the G88S mutation appears to be at the extreme end of the severity spectrum, particularly for its devastating effect on CYP21A2 activity, which was reduced to a mere 1.3% of wild-type activity, compared to the 4% reported for L374H. Deficiency in CYP21A2 is the hallmark of classic congenital adrenal hyperplasia (CAH), characterized by impaired cortisol synthesis and a compensatory increase in ACTH secretion, leading to adrenal hyperplasia and excessive progesterone and 17OHP production. The severe impact of the G88S mutation on CYP21A2 activity likely accounts for the significant features of CAH often observed in patients with POR deficiency [40,57,105,106]. The more severe impact of POR G88S on CYP21A2 (1.3% activity) versus CYP17A1 (5.5% activity) despite a global mechanism of protein instability, suggests that the residual, partially functional POR protein has a conformation that is particularly inept at supporting CYP21A2. It is established that different POR mutations can selectively impact partner enzymes; for instance, the common A287P variant preferentially inhibits CYP17A1 while retaining near-normal CYP21A2 activity. This highlights that the structural and dynamic requirements for each POR-P450 partnership are unique and highly specific. It can be hypothesized that the G88S-induced instability and conformational changes are exceptionally disruptive to the specific protein-protein interface or electron transfer dynamics required by CYP21A2, providing a direct molecular basis for the prominent congenital adrenal hyperplasia phenotype seen in all affected patients. The severe loss of steroid metabolizing enzyme activities, positions G88S as one of the most severe *POR* mutations described to date, establishing a new benchmark for the severity of a single homozygous mutation.

The in-depth functional characterization of the G88S POR variant extends beyond steroidogenesis to reveal serious implications for drug metabolism, a finding that has immediate and critical clinical relevance. The in vitro assays demonstrated that the G88S mutation severely impaired the activities of four major drug-metabolizing enzymes: CYP3A4, CYP3A5, CYP2C9, and CYP2C19. The activity supported by the G88S variant for each of these enzymes was reduced to a single-digit percentage of WT levels: 3.3% for CYP3A4, 9% for CYP3A5, 3% for CYP2C9, and 4% for CYP2C19.

A critical finding with immediate clinical relevance is that the G88S mutation creates a ‘poor metabolizer’ phenotype, with residual activity for major drug-metabolizing enzymes like CYP3A4 and CYP2C9 falling to just 3-9% of wild-type levels. While no overt clinical evidence of adverse drug reactions (ADRs) was observed in this pediatric cohort, this is not unexpected given their young age and likely limited exposure to medications metabolized by these pathways. The absence of observed ADRs should not be interpreted as an absence of risk; rather, it underscores the profound importance of our in vitro findings as a preemptive pharmacogenomic warning. Studies in adult patients with other POR mutations have confirmed that such defects lead to impaired in vivo drug metabolism. For patients with the G88S mutation, standard doses of common drugs such as warfarin (CYP2C9), certain proton pump inhibitors (CYP2C19), or the vast number of prescription drugs metabolized by CYP3A4 could lead to severe toxicity. Therefore, the identification of this mutation is not merely a diagnostic tool for their endocrine condition but an essential, lifelong guide for personalized pharmacotherapy, mandating careful drug selection and dose adjustment to prevent future harm.

Conclusion

The characterization of the G88S mutation in POR represents a significant advancement in the understanding of P450 oxidoreductase deficiency (Table 5). The in vitro functional assays, combined with molecular modeling, revealed a novel molecular pathomechanism: the G88S substitution causes a dynamic protein instability, leading to the catastrophic loss of both FMN and FAD cofactors. This

 doi:10.20944/preprints202510.0422.v1

widespread structural defect is the direct cause of the near-complete loss of enzymatic activity, particularly the devastating effect on CYP21A2, which was reduced to a mere 1.3% of wild-type function. This positions G88S as one of the most severe POR mutations described to date and provides a direct molecular link to the prominent congenital adrenal hyperplasia phenotype observed in all affected patients.

Table 5. Summary of Molecular, Functional, and Clinical Correlations of the *POR* G88S Mutation.

Molecular Finding	In Vitro Functional Consequence	Clinical/Biochemical Phenotype
Homozygous G88S mutation in FMN domain	Catastrophic loss of FMN and FAD (<30, <15%) due to dynamic protein instability	Severe P450 Oxidoreductase Deficiency (PORD)
	CYP21A2 (21-hydroxylase) activity at 1.3% of WT	**Congenital Adrenal Hyperplasia:** High 17OHP & Progesterone; Low/inadequate Cortisol; High ACTH
	CYP17A1 (17,20-lyase) activity at 5.5% of WT	**Gonadal Dysfunction:** 46,XY undervirilization (impaired Testosterone); 46,XX delayed puberty (impaired Estradiol)
	CYP3A4/5, 2C9, 2C19 activity at 3-9% of WT	**Lifelong Pharmacogenomic Risk:** "Pan-poor metabolizer" phenotype; High risk of adverse drug reactions (ADRs)
	Variable (Modifier	

The analysis of the clinical presentation further revealed a critical genotype-phenotype discrepancy. The identification of four individuals with an identical homozygous G88S mutation, but with only one of them presenting the full skeletal features of Antley-Bixler Syndrome, indicates that the G88S mutation is necessary for the biochemical defect but not sufficient for the full skeletal phenotype. This strongly suggests that other genetic, epigenetic, or environmental factors are at play, modulating the clinical expression of the disease. Additionally, the case of the 46,XX patient with delayed puberty, rather than virilization, provides a new perspective on the clinical spectrum of PORD, demonstrating how the severity of a specific mutation can completely alter the expected phenotype by impairing key steroidogenic enzymes.

Beyond the established endocrinological effects, the findings on drug metabolism are of immediate and critical clinical utility. The G88S mutation effectively creates a "pan-poor metabolizer" phenotype for a vast range of commonly prescribed drugs by severely compromising the activities of CYP3A4, CYP3A5, CYP2C9, and CYP2C19. This information transforms POR from a gene of academic interest into a critical pharmacogenomic marker.

The characterization of the *POR* G88S mutation provides a clear example of translational medicine, linking a specific molecular defect to a severe clinical syndrome and a critical, lifelong pharmacogenomic risk profile. Based on these findings, genotyping for this specific variant should be considered in at-risk populations, such as Argentine newborns with DSD or suspected CAH. Early identification would not only enable timely and appropriate hormone replacement but would also allow for the entry of a preemptive pharmacogenomic warning into the patient's medical record. Future management of these individuals must involve close collaboration between endocrinologists and clinical pharmacologists. Further research should focus on developing a functional 'activity score' for different POR variants against a panel of key P450 enzymes, creating a more nuanced

 doi:10.20944/preprints202510.0422.v1

predictive tool for both steroidogenic and drug-metabolizing capacity. Such an approach would pave the way for truly personalized medicine for all individuals living with PORD.

Acknowledgments: This work was supported by grants from the Swiss National Science Foundation (204518 and 229294), EU COST Action CA21162 (COZYME), the Novartis Foundation for Medical-Biological Research (18A053) and Burgergemiende Bern to AVP, and from Fondo Argentino Sectorial (FONARSEC, Argentina) grant numbers FS-BIO 05/2017 and PICT-A Cat.III 73/2021 to RAR and MGR. MNRV and KS were funded in part by the SWISS GOVERNMENT EXCELLENCE SCHOLARSHIP (ESKAS) grants, 2020.0557 and 2019.0385.

References

1. Pandey, A. V.; Flück, C. E., NADPH P450 oxidoreductase: structure, function, and pathology of diseases. *Pharmacol Ther* **2013,** 138, (2), 229-54.
2. Flück, C. E.; Tajima, T.; Pandey, A. V.; Arlt, W.; Okuhara, K.; Verge, C. F.; Jabs, E. W.; Mendonça, B. B.; Fujieda, K.; Miller, W. L., Mutant P450 oxidoreductase causes disordered steroidogenesis with and without Antley-Bixler syndrome. *Nat Genet* **2004,** 36, (3), 228-30.
3. Miller, W. L.; Huang, N.; Flück, C. E.; Pandey, A. V., P450 oxidoreductase deficiency. *Lancet* **2004,** 364, (9446), 1663.
4. Pandey, A. V.; Fluck, C. E.; Huang, N.; Tajima, T.; Fujieda, K.; Miller, W. L., P450 oxidoreductase deficiency: a new disorder of steroidogenesis affecting all microsomal P450 enzymes. *Endocr Res* **2004,** 30, (4), 881-8.
5. Adachi, M.; Tachibana, K.; Asakura, Y.; Yamamoto, T.; Hanaki, K.; Oka, A., Compound heterozygous mutations of cytochrome P450 oxidoreductase gene (POR) in two patients with Antley-Bixler syndrome. *Am J Med Genet A* **2004,** 128A, (4), 333-9.
6. Arlt, W.; Walker, E. A.; Draper, N.; Ivison, H. E.; Ride, J. P.; Hammer, F.; Chalder, S. M.; Borucka-Mankiewicz, M.; Hauffa, B. P.; Malunowicz, E. M.; Stewart, P. M.; Shackleton, C. H., Congenital adrenal hyperplasia caused by mutant P450 oxidoreductase and human androgen synthesis: analytical study. *Lancet* **2004,** 363, (9427), 2128-35.
7. Fukami, M.; Horikawa, R.; Nagai, T.; Tanaka, T.; Naiki, Y.; Sato, N.; Okuyama, T.; Nakai, H.; Soneda, S.; Tachibana, K.; Matsuo, N.; Sato, S.; Homma, K.; Nishimura, G.; Hasegawa, T.; Ogata, T., Cytochrome P450 oxidoreductase gene mutations and Antley-Bixler syndrome with abnormal genitalia and/or impaired steroidogenesis: Molecular and clinical studies in 10 patients. *J Clin Endocr Metab* **2005,** 90, (1), 414-426.
8. Huang, N.; Pandey, A. V.; Agrawal, V.; Reardon, W.; Lapunzina, P. D.; Mowat, D.; Jabs, E. W.; Van Vliet, G.; Sack, J.; Flück, C. E.; Miller, W. L., Diversity and function of mutations in p450 oxidoreductase in patients with Antley-Bixler syndrome and disordered steroidogenesis. *Am J Hum Genet* **2005,** 76, (5), 729-49.
9. Adachi, M.; Asakura, Y.; Matsuo, M.; Yamamoto, T.; Hanaki, K.; Arlt, W., POR R457H is a global founder mutation causing Antley-Bixler syndrome with autosomal recessive trait. *Am J Med Genet A* **2006,** 140, (6), 633-5.
10. Fukami, M.; Hasegawa, T.; Horikawa, R.; Ohashi, T.; Nishimura, G.; Homma, K.; Ogata, T., Cytochrome P450 oxidoreductase deficiency in three patients initially regarded as having 21-hydroxylase deficiency and/or aromatase deficiency: Diagnostic value of urine steroid hormone analysis. *Pediatric Research* **2006,** 59, (2), 276-280.
11. Homma, K.; Hasegawa, T.; Nagai, T.; Adachi, M.; Horikawa, R.; Fujiwara, I.; Tajima, T.; Takeda, R.; Fukami, M.; Ogata, T., Urine steroid hormone profile analysis in cytochrome P450 oxidoreductase deficiency: Implication for the backdoor pathway to dihydrotestosterone. *J Clin Endocr Metab* **2006,** 91, (7), 2643-2649.
12. Lu, A. Y. H.; Junk, K. W.; Coon, M. J., Resolution of Cytochrome P-450-Containing Omega-Hydroxylation System of Liver Microsomes into 3 Components. *Journal of Biological Chemistry* **1969,** 244, (13), 3714-+.
13. Guengerich, F. P.; Ballou, D. P.; Coon, M. J., Purified liver microsomal cytochrome P-450. Electron-accepting properties and oxidation-reduction potential. *J Biol Chem* **1975,** 250, (18), 7405-14.
14. Lu, A. Y.; Junk, K. W.; Coon, M. J., Resolution of the cytochrome P-450-containing omega-hydroxylation system of liver microsomes into three components. *J Biol Chem* **1969,** 244, (13), 3714-21.

 doi:10.20944/preprints202510.0422.v1

15. Guengerich, F. P., Reduction of cytochrome b(5) by NADPH-cytochrome P450 reductase. *Archives of Biochemistry and Biophysics* **2005,** 440, (2), 204-211.
16. Masters, B. S.; Nelson, E. B.; Schacter, B. A.; Baron, J.; Isaacson, E. L., NADPH-cytochrome c reductase and its role in microsomal cytochrome P-450-dependent reactions. *Drug Metab Dispos* **1973,** 1, (1), 121-8.
17. Nelson, E. B.; Kohl, K. B.; Masters, B. S., The role of NADPH-cytochrome c reductase in the microsomal oxidation of ethanol and methanol. *Drug Metab Dispos* **1973,** 1, (1), 455-60.
18. Yasukochi, Y.; Masters, B. S., Some properties of a detergent-solubilized NADPH-cytochrome c(cytochrome P-450) reductase purified by biospecific affinity chromatography. *J Biol Chem* **1976,** 251, (17), 5337-44.
19. Prough, R. A.; Masters, B. S., The mechanism of cytochrome b5 reduction by NADPH-cytochrome c reductase. *Arch Biochem Biophys* **1974,** 165, (1), 263-7.
20. Schacter, B. A.; Nelson, E. B.; Marver, H. S.; Masters, B. S., Immunochemical evidence for an association of heme oxygenase with the microsomal electron transport system. *J Biol Chem* **1972,** 247, (11), 3601-7.
21. Bligh, H. F.; Bartoszek, A.; Robson, C. N.; Hickson, I. D.; Kasper, C. B.; Beggs, J. D.; Wolf, C. R., Activation of mitomycin C by NADPH:cytochrome P-450 reductase. *Cancer Res* **1990,** 50, (24), 7789-92.
22. Bartoszek, A.; Wolf, C. R., Enhancement of Doxorubicin Toxicity Following Activation by Nadph Cytochrome P450 Reductase. *Biochemical Pharmacology* **1992,** 43, (7), 1449-1457.
23. Walton, M. I.; Wolf, C. R.; Workman, P., The Role of Cytochrome-P450 and Cytochrome-P450 Reductase in the Reductive Bioactivation of the Novel Benzotriazine Di-N-Oxide Hypoxic Cytotoxin 3-Amino-1,2,4-Benzotriazine-1,4-Dioxide (Sr-4233, Win-59075) by Mouse-Liver. *Biochemical Pharmacology* **1992,** 44, (2), 251-259.
24. Wu, L.; Gu, J.; Weng, Y.; Kluetzman, K.; Swiatek, P.; Behr, M.; Zhang, Q. Y.; Zhuo, X.; Xie, Q.; Ding, X., Conditional knockout of the mouse NADPH-cytochrome p450 reductase gene. *Genesis* **2003,** 36, (4), 177-81.
25. Gu, J.; Weng, Y.; Zhang, Q. Y.; Cui, H. D.; Behr, M.; Wu, L.; Yang, W. Z.; Zhang, L.; Ding, X. X., Liver-specific deletion of the NADPH-cytochrome P450 reductase gene–Impact on plasma cholesterol homeostasis and the function and regulation of microsomal cytochrome P450 and heme oxygenase. *Journal of Biological Chemistry* **2003,** 278, (28), 25895-25901.
26. Henderson, C. J.; Otto, D. M. E.; Carrie, D.; Magnuson, M. A.; McLaren, A. W.; Rosewell, I.; Wolf, C. R., Inactivation of the hepatic cytochrome P450 system by conditional deletion of hepatic cytochrome P450 reductase. *Journal of Biological Chemistry* **2003,** 278, (15), 13480-13486.
27. Henderson, C. J.; Otto, D. M. E.; Carrie, D.; McLaren, A. W.; Ross, J.; Rosewell, I.; Wolf, C. R., Mouse hepatic P450 reductase knockout. *Toxicology* **2004,** 194, (3), 216-217.
28. Weng, Y.; DiRusso, C. C.; Reilly, A. A.; Black, P. N.; Ding, X. X., Hepatic gene expression changes in mouse models with liver-specific deletion or global suppression of the NADPH-cytochrome P450 reductase gene–Mechanistic implications for the regulation of microsomal cytochrome P450 and the fatty liver phenotype. *Journal of Biological Chemistry* **2005,** 280, (36), 31686-31698.
29. Gu, J.; Wu, L.; Weng, Y.; Kluetzman, K.; Cui, H. D.; Zhang, Q. Y.; Yang, W. Z.; Ding, X. X., Preparation and characterization of mice with liver-specific deletion of the NADPH-cytochrome P-450 reductase gene. *Drug Metabolism Reviews* **2002,** 34, 112-112.
30. Gu, J.; Chen, C. S.; Wei, Y.; Fang, C.; Xie, F.; Kannan, K.; Yang, W. Z.; Waxman, D. J.; Ding, X. X., A mouse model with liver-specific deletion and global suppression of the NADPH-Cytochrome P450 reductase gene: Characterization and utility for in vivo studies of cyclophosphamide disposition. *Journal of Pharmacology and Experimental Therapeutics* **2007,** 321, (1), 9-17.
31. Parween, S.; Fernandez-Cancio, M.; Benito-Sanz, S.; Camats, N.; Rojas Velazquez, M. N.; Lopez-Siguero, J. P.; Udhane, S. S.; Kagawa, N.; Fluck, C. E.; Audi, L.; Pandey, A. V., Molecular Basis of CYP19A1 Deficiency in a 46,XX Patient With R550W Mutation in POR: Expanding the PORD Phenotype. *J Clin Endocrinol Metab* **2020,** 105, (4), dgaa076.
32. Parween, S.; Roucher-Boulez, F.; Flück, C. E.; Lienhardt-Roussie, A.; Mallet, D.; Morel, Y.; Pandey, A. V., P450 Oxidoreductase Deficiency: Loss of Activity Caused by Protein Instability From a Novel L374H Mutation. *J Clin Endocrinol Metab* **2016,** 101, (12), 4789-4798.

 doi:10.20944/preprints202510.0422.v1

33. Flück, C. E.; Mallet, D.; Hofer, G.; Samara-Boustani, D.; Leger, J.; Polak, M.; Morel, Y.; Pandey, A. V., Deletion of P399_E401 in NADPH cytochrome P450 oxidoreductase results in partial mixed oxidase deficiency. *Biochem Biophys Res Commun* **2011,** 412, (4), 572-7.
34. Jensen, S. B.; Thodberg, S.; Parween, S.; Moses, M. E.; Hansen, C. C.; Thomsen, J.; Sletfjerding, M. B.; Knudsen, C.; Del Giudice, R.; Lund, P. M.; Castano, P. R.; Bustamante, Y. G.; Velazquez, M. N. R.; Jorgensen, F. S.; Pandey, A. V.; Laursen, T.; Moller, B. L.; Hatzakis, N. S., Biased cytochrome P450-mediated metabolism via small-molecule ligands binding P450 oxidoreductase. *Nat Commun* **2021,** 12, (1), 2260.
35. Riddick, D. S.; Ding, X.; Wolf, C. R.; Porter, T. D.; Pandey, A. V.; Zhang, Q. Y.; Gu, J.; Finn, R. D.; Ronseaux, S.; McLaughlin, L. A.; Henderson, C. J.; Zou, L.; Flück, C. E., NADPH-cytochrome P450 oxidoreductase: roles in physiology, pharmacology, and toxicology. *Drug Metab Dispos* **2013,** 41, (1), 12-23.
36. Kamin, H.; Masters, B. S.; Gibson, Q. H.; Williams, C. H., Jr., Microsomal TPNH-cytochrome c reductase. *Fed Proc* **1965,** 24, (5), 1164-71.
37. Masters, B. S.; Okita, R. T., The history, properties, and function of NADPH-cytochrome P-450 reductase. *Pharmacol Ther* **1980,** 9, (2), 227-44.
38. Rojas Velazquez, M. N.; Therkelsen, S.; Pandey, A. V., Exploring Novel Variants of the Cytochrome P450 Reductase Gene (POR) from the Genome Aggregation Database by Integrating Bioinformatic Tools and Functional Assays. *Biomolecules* **2023,** 13, (12), 1728.
39. Burkhard, F. Z.; Parween, S.; Udhane, S. S.; Flück, C. E.; Pandey, A. V., P450 Oxidoreductase deficiency: Analysis of mutations and polymorphisms. *J Steroid Biochem Mol Biol* **2017,** 165, (Pt A), 38-50.
40. Scott, R. R.; Gomes, L. G.; Huang, N.; Van Vliet, G.; Miller, W. L., Apparent manifesting heterozygosity in P450 oxidoreductase deficiency and its effect on coexisting 21-hydroxylase deficiency. *J Clin Endocrinol Metab* **2007,** 92, (6), 2318-22.
41. Gomes, L. G.; Huang, N.; Agrawal, V.; Mendonca, B. B.; Bachega, T. A.; Miller, W. L., The common P450 oxidoreductase variant A503V is not a modifier gene for 21-hydroxylase deficiency. *J Clin Endocrinol Metab* **2008,** 93, (7), 2913-6.
42. Hershkovitz, E.; Parvari, R.; Wudy, S. A.; Hartmann, M. F.; Gomes, L. G.; Loewental, N.; Miller, W. L., Homozygous mutation G539R in the gene for P450 oxidoreductase in a family previously diagnosed as having 17,20-lyase deficiency. *J Clin Endocr Metab* **2008,** 93, (9), 3584-3588.
43. Sahakitrungruang, T.; Huang, N.; Tee, M. K.; Agrawal, V.; Russell, W. E.; Crock, P.; Murphy, N.; Migeon, C. J.; Miller, W. L., Clinical, genetic, and enzymatic characterization of P450 oxidoreductase deficiency in four patients. *J Clin Endocrinol Metab* **2009,** 94, (12), 4992-5000.
44. Marohnic, C. C.; Panda, S. P.; Martasek, P.; Masters, B. S., Diminished FAD binding in the Y459H and V492E Antley-Bixler syndrome mutants of human cytochrome P450 reductase. *J Biol Chem* **2006,** 281, (47), 35975-82.
45. Marohnic, C. C.; Panda, S. P.; McCammon, K.; Rueff, J.; Masters, B. S. S.; Kranendonk, M., Human Cytochrome P450 Oxidoreductase Deficiency Caused by the Y181D Mutation: Molecular Consequences and Rescue of Defect. *Drug Metabolism and Disposition* **2010,** 38, (2), 332-340.
46. Pandey, A. V.; Sproll, P., Pharmacogenomics of human P450 oxidoreductase. *Front Pharmacol* **2014,** 5, 103.
47. Nicolo, C.; Flück, C. E.; Mullis, P. E.; Pandey, A. V., Restoration of mutant cytochrome P450 reductase activity by external flavin. *Mol Cell Endocrinol* **2010,** 321, (2), 245-52.
48. Rojas Velazquez, M. N.; Noebauer, M.; Pandey, A. V., Loss of Protein Stability and Function Caused by P228L Variation in NADPH-Cytochrome P450 Reductase Linked to Lower Testosterone Levels. *International journal of molecular sciences* **2022,** 23, (17), 10141.
49. McCammon, K. M.; Panda, S. P.; Xia, C.; Kim, J. J.; Moutinho, D.; Kranendonk, M.; Auchus, R. J.; Lafer, E. M.; Ghosh, D.; Martasek, P.; Kar, R.; Masters, B. S.; Roman, L. J., Instability of the Human Cytochrome P450 Reductase A287P Variant Is the Major Contributor to Its Antley-Bixler Syndrome-like Phenotype. *J Biol Chem* **2016,** 291, (39), 20487-502.
50. Campelo, D.; Lautier, T.; Urban, P.; Esteves, F.; Bozonnet, S.; Truan, G.; Kranendonk, M., The Hinge Segment of Human NADPH-Cytochrome P450 Reductase in Conformational Switching: The Critical Role of Ionic Strength. *Front Pharmacol* **2017,** 8, 755.

 doi:10.20944/preprints202510.0422.v1

51. Campelo, D.; Esteves, F.; Brito Palma, B.; Costa Gomes, B.; Rueff, J.; Lautier, T.; Urban, P.; Truan, G.; Kranendonk, M., Probing the Role of the Hinge Segment of Cytochrome P450 Oxidoreductase in the Interaction with Cytochrome P450. *International Journal of Molecular Sciences* **2018,** 19, (12), 3914.
52. Porter, T. D.; Kasper, C. B., NADPH-cytochrome P-450 oxidoreductase: flavin mononucleotide and flavin adenine dinucleotide domains evolved from different flavoproteins. *Biochemistry* **1986,** 25, (7), 1682-7.
53. Porter, T. D.; Kasper, C. B., Coding nucleotide sequence of rat NADPH-cytochrome P-450 oxidoreductase cDNA and identification of flavin-binding domains. *Proc Natl Acad Sci U S A* **1985,** 82, (4), 973-7.
54. Xia, C.; Hamdane, D.; Shen, A. L.; Choi, V.; Kasper, C. B.; Pearl, N. M.; Zhang, H.; Im, S. C.; Waskell, L.; Kim, J. J., Conformational changes of NADPH-cytochrome P450 oxidoreductase are essential for catalysis and cofactor binding. *J Biol Chem* **2011,** 286, (18), 16246-60.
55. Hubbard, P. A.; Shen, A. L.; Paschke, R.; Kasper, C. B.; Kim, J. J., NADPH-cytochrome P450 oxidoreductase. Structural basis for hydride and electron transfer. *J Biol Chem* **2001,** 276, (31), 29163-70.
56. Fluck, C. E.; Parween, S.; Rojas Velazquez, M. N.; Pandey, A. V., Inhibition of placental CYP19A1 activity remains as a valid hypothesis for 46,XX virilization in P450 oxidoreductase deficiency. *Proc Natl Acad Sci U S A* **2020,** 117, (26), 14632-14633.
57. Flück, C. E.; Rojas Velazquez, M. N.; Pandey, A. V., Chapter 12–P450 oxidoreductase deficiency. In *Genetic Steroid Disorders (Second Edition)*, New, M. I., Ed. Academic Press: San Diego, 2023; pp 239-264.
58. Lejarraga, H.; Orfila, G., Estándares de peso y estatura para niñas y niños argentinos desde el nacimiento hasta la madurez. *Arch.Argent.Pediatr.* **1987,** 85, 209-213.
59. van der Straaten, S.; Springer, A.; Zecic, A.; Hebenstreit, D.; Tonnhofer, U.; Gawlik, A.; Baumert, M.; Szeliga, K.; Debulpaep, S.; Desloovere, A.; Tack, L.; Smets, K.; Wasniewska, M.; Corica, D.; Calafiore, M.; Ljubicic, M. L.; Busch, A. S.; Juul, A.; Nordenstrom, A.; Sigurdsson, J.; Fluck, C. E.; Haamberg, T.; Graf, S.; Hannema, S. E.; Wolffenbuttel, K. P.; Hiort, O.; Ahmed, S. F.; Cools, M., The External Genitalia Score (EGS): A European Multicenter Validation Study. *J Clin Endocrinol Metab* **2020,** 105, (3), e222-e230.
60. Marshall, W. A.; Tanner, J. M., Variations in the pattern of pubertal changes in boys. *Archives of Disease in Childhood* **1970,** 45, (239), 13-23.
61. Anigstein, C. R., Longitud y diámetro del pene en niños de 0 a 14 años de edad. *Arch.Argent.Pediatr.* **2005,** 103, (5), 401-405.
62. Ballerini, M. G.; Chiesa, A.; Morelli, C.; Frusti, M.; Ropelato, M. G., Serum concentration of 17alpha-hydroxyprogesterone in children from birth to adolescence. *Hormone research in paediatrics* **2014,** 81, (2), 118-25.
63. Ballerini, M. G.; Gaido, V.; Rodriguez, M. E.; Chiesa, A.; Ropelato, M. G., Prospective and Descriptive Study on Serum Androstenedione Concentration in Healthy Children from Birth until 18 Years of Age and Its Associated Factors. *Dis Markers* **2017,** 2017, 9238304.
64. Bergadá, I.; Milani, C.; Bedecarrás, P.; Andreone, L.; Ropelato, M. G.; Gottlieb, S.; Bergadá, C.; Campo, S.; Rey, R. A., Time course of the serum gonadotropin surge, inhibins, and anti-Mullerian hormone in normal newborn males during the first month of life. *J Clin Endocrinol Metab* **2006,** 91, (10), 4092-8.
65. Grinspon, R. P.; Bedecarrás, P.; Ballerini, M. G.; Iñíguez, G.; Rocha, A.; Mantovani Rodrigues Resende, E. A.; Brito, V. N.; Milani, C.; Figueroa Gacitua, V.; Chiesa, A.; Keselman, A.; Gottlieb, S.; Borges, M. F.; Ropelato, M. G.; Picard, J. Y.; Codner, E.; Rey, R. A., Early onset of primary hypogonadism revealed by serum anti-Müllerian hormone determination during infancy and childhood in trisomy 21. *International Journal of Andrology* **2011,** 34, (5 Pt 2), e487-e498.
66. Saez, J. M.; Bertrand, J., Studies on testicular function in children: plasma concentrations of testosterone, dehydroepiandrosterone and its sulfate before and after stimulation with human chorionic gonadotrophin. (1). *Steroids* **1968,** 12, (6), 749-61.

 doi:10.20944/preprints202510.0422.v1

67. Grinspon, R. P.; Ropelato, M. G.; Gottlieb, S.; Keselman, A.; Martínez, A.; Ballerini, M. G.; Domené, H. M.; Rey, R. A., Basal follicle-stimulating hormone and peak gonadotropin levels after gonadotropin-releasing hormone infusion show high diagnostic accuracy in boys with suspicion of hypogonadotropic hypogonadism. *J Clin Endocrinol Metab* **2010,** 95, (6), 2811-8.
68. Karczewski, K. J.; Francioli, L. C.; Tiao, G.; Cummings, B. B.; Alfoldi, J.; Wang, Q.; Collins, R. L.; Laricchia, K. M.; Ganna, A.; Birnbaum, D. P.; Gauthier, L. D.; Brand, H.; Solomonson, M.; Watts, N. A.; Rhodes, D.; Singer-Berk, M.; England, E. M.; Seaby, E. G.; Kosmicki, J. A.; Walters, R. K.; Tashman, K.; Farjoun, Y.; Banks, E.; Poterba, T.; Wang, A.; Seed, C.; Whiffin, N.; Chong, J. X.; Samocha, K. E.; Pierce-Hoffman, E.; Zappala, Z.; O'Donnell-Luria, A. H.; Minikel, E. V.; Weisburd, B.; Lek, M.; Ware, J. S.; Vittal, C.; Armean, I. M.; Bergelson, L.; Cibulskis, K.; Connolly, K. M.; Covarrubias, M.; Donnelly, S.; Ferriera, S.; Gabriel, S.; Gentry, J.; Gupta, N.; Jeandet, T.; Kaplan, D.; Llanwarne, C.; Munshi, R.; Novod, S.; Petrillo, N.; Roazen, D.; Ruano-Rubio, V.; Saltzman, A.; Schleicher, M.; Soto, J.; Tibbetts, K.; Tolonen, C.; Wade, G.; Talkowski, M. E.; Genome Aggregation Database, C.; Neale, B. M.; Daly, M. J.; MacArthur, D. G., The mutational constraint spectrum quantified from variation in 141,456 humans. *Nature* **2020,** 581, (7809), 434-443.
69. Li, Q.; Wang, K., InterVar: Clinical Interpretation of Genetic Variants by the 2015 ACMG-AMP Guidelines. *Am J Hum Genet* **2017,** 100, (2), 267-280.
70. Landrum, M. J.; Lee, J. M.; Benson, M.; Brown, G. R.; Chao, C.; Chitipiralla, S.; Gu, B.; Hart, J.; Hoffman, D.; Jang, W.; Karapetyan, K.; Katz, K.; Liu, C.; Maddipatla, Z.; Malheiro, A.; McDaniel, K.; Ovetsky, M.; Riley, G.; Zhou, G.; Holmes, J. B.; Kattman, B. L.; Maglott, D. R., ClinVar: improving access to variant interpretations and supporting evidence. *Nucleic Acids Res* **2018,** 46, (D1), D1062-D1067.
71. Kitts, A.; Phan, L.; Ward, M.; Holmes, J. B., *The Database of Short Genetic Variation (dbSNP)*. 2nd. Ed ed.; National Center for Biotechnology Information: Bethesda, MD (USA), 2019.
72. Buniello, A.; MacArthur, J. A. L.; Cerezo, M.; Harris, L. W.; Hayhurst, J.; Malangone, C.; McMahon, A.; Morales, J.; Mountjoy, E.; Sollis, E.; Suveges, D.; Vrousgou, O.; Whetzel, P. L.; Amode, R.; Guillen, J. A.; Riat, H. S.; Trevanion, S. J.; Hall, P.; Junkins, H.; Flicek, P.; Burdett, T.; Hindorff, L. A.; Cunningham, F.; Parkinson, H., The NHGRI-EBI GWAS Catalog of published genome-wide association studies, targeted arrays and summary statistics 2019. *Nucleic Acids Res* **2019,** 47, (D1), D1005-D1012.
73. Fowler, A.; Mahamdallie, S.; Ruark, E.; Seal, S.; Ramsay, E.; Clarke, M.; Uddin, I.; Wylie, H.; Strydom, A.; Lunter, G.; Rahman, N., Accurate clinical detection of exon copy number variants in a targeted NGS panel using DECoN. *Wellcome Open Res* **2016,** 1, 20.
74. Pandey, A. V.; Kempna, P.; Hofer, G.; Mullis, P. E.; Flück, C. E., Modulation of human CYP19A1 activity by mutant NADPH P450 oxidoreductase. *Mol Endocrinol* **2007,** 21, (10), 2579-95.
75. Pandey, A. V.; Flück, C. E.; Mullis, P. E., Altered heme catabolism by heme oxygenase-1 caused by mutations in human NADPH cytochrome P450 reductase. *Biochem Biophys Res Commun* **2010,** 400, (3), 374-8.
76. Parween, S.; Rojas Velazquez, M. N.; Udhane, S. S.; Kagawa, N.; Pandey, A. V., Variability in Loss of Multiple Enzyme Activities Due to the Human Genetic Variation P284T Located in the Flexible Hinge Region of NADPH Cytochrome P450 Oxidoreductase. *Frontiers in Pharmacology* **2019,** 10, 1187.
77. Faeder, E. J.; Siegel, L. M., A rapid micromethod for determination of FMN and FAD in mixtures. *Anal Biochem* **1973,** 53, (1), 332-6.
78. Pandey, A. V.; Miller, W. L., Regulation of 17,20 lyase activity by cytochrome b5 and by serine phosphorylation of P450c17. *J Biol Chem* **2005,** 280, (14), 13265-71.
79. Pandey, A. V.; Mellon, S. H.; Miller, W. L., Protein phosphatase 2A and phosphoprotein SET regulate androgen production by P450c17. *J Biol Chem* **2003,** 278, (5), 2837-44.
80. Yakubu, J.; Natsaridis, E.; du Toit, T.; Barata, I. S.; Tagit, O.; Pandey, A. V., Nanoparticles with curcumin and piperine modulate steroid biosynthesis in prostate cancer. *Sci Rep* **2025,** 15, (1), 13613.
81. Wrobel, T. M.; Grudzinska, A.; Yakubu, J.; du Toit, T.; Sharma, K.; Harrington, J. C.; Bjorkling, F.; Jorgensen, F. S.; Pandey, A. V., Pyridine indole hybrids as novel potent CYP17A1 inhibitors. *J Enzyme Inhib Med Chem* **2025,** 40, (1), 2463014.

 doi:10.20944/preprints202510.0422.v1

82. Wrobel, T. M.; Sharma, K.; Mannella, I.; Oliaro-Bosso, S.; Nieckarz, P.; Du Toit, T.; Voegel, C. D.; Rojas Velazquez, M. N.; Yakubu, J.; Matveeva, A.; Therkelsen, S.; Jorgensen, F. S.; Pandey, A. V.; Pippione, A. C.; Lolli, M. L.; Boschi, D.; Bjorkling, F., Exploring the Potential of Sulfur Moieties in Compounds Inhibiting Steroidogenesis. *Biomolecules* **2023,** 13, (9), 1349.
83. Wrobel, T. M.; Rogova, O.; Sharma, K.; Rojas Velazquez, M. N.; Pandey, A. V.; Jorgensen, F. S.; Arendrup, F. S.; Andersen, K. L.; Bjorkling, F., Synthesis and Structure-Activity Relationships of Novel Non-Steroidal CYP17A1 Inhibitors as Potential Prostate Cancer Agents. *Biomolecules* **2022,** 12, (2), 165.
84. Sharma, K.; Lanzilotto, A.; Yakubu, J.; Therkelsen, S.; Voegel, C. D.; Du Toit, T.; Jorgensen, F. S.; Pandey, A. V., Effect of Essential Oil Components on the Activity of Steroidogenic Cytochrome P450. *Biomolecules* **2024,** 14, (2), 203.
85. Prado, M. J.; Singh, S.; Ligabue-Braun, R.; Meneghetti, B. V.; Rispoli, T.; Kopacek, C.; Monteiro, K.; Zaha, A.; Rossetti, M. L. R.; Pandey, A. V., Characterization of Mutations Causing CYP21A2 Deficiency in Brazilian and Portuguese Populations. *Int J Mol Sci* **2021,** 23, (1), 296.
86. Malikova, J.; Brixius-Anderko, S.; Udhane, S. S.; Parween, S.; Dick, B.; Bernhardt, R.; Pandey, A. V., CYP17A1 inhibitor abiraterone, an anti-prostate cancer drug, also inhibits the 21-hydroxylase activity of CYP21A2. *J Steroid Biochem Mol Biol* **2017,** 174, 192-200.
87. Udhane, S. S.; Dick, B.; Hu, Q.; Hartmann, R. W.; Pandey, A. V., Specificity of anti-prostate cancer CYP17A1 inhibitors on androgen biosynthesis. *Biochem Biophys Res Commun* **2016,** 477, (4), 1005-10.
88. Velazquez, M. N. R.; Parween, S.; Udhane, S. S.; Pandey, A. V., Variability in human drug metabolizing cytochrome P450 CYP2C9, CYP2C19 and CYP3A5 activities caused by genetic variations in cytochrome P450 oxidoreductase. *Biochem Biophys Res Commun* **2019,** 515, (1), 133-138.
89. Parween, S.; Rojas Velazquez, M. N.; Udhane, S. S.; Kagawa, N.; Pandey, A. V., Variability in Loss of Multiple Enzyme Activities Due to the Human Genetic Variation P284T Located in the Flexible Hinge Region of NADPH Cytochrome P450 Oxidoreductase. *Front Pharmacol* **2019,** 10, 1187.
90. Udhane, S. S.; Parween, S.; Kagawa, N.; Pandey, A. V., Altered CYP19A1 and CYP3A4 Activities Due to Mutations A115V, T142A, Q153R and P284L in the Human P450 Oxidoreductase. *Front Pharmacol* **2017,** 8, 580.
91. Parween, S.; DiNardo, G.; Baj, F.; Zhang, C.; Gilardi, G.; Pandey, A. V., Differential effects of variations in human P450 oxidoreductase on the aromatase activity of CYP19A1 polymorphisms R264C and R264H. *J Steroid Biochem Mol Biol* **2020,** 196, 105507.
92. Xia, C.; Panda, S. P.; Marohnic, C. C.; Martasek, P.; Masters, B. S.; Kim, J. J., Structural basis for human NADPH-cytochrome P450 oxidoreductase deficiency. *Proc Natl Acad Sci U S A* **2011,** 108, (33), 13486-91.
93. Hamdane, D.; Xia, C. W.; Im, S. C.; Zhang, H. M.; Kim, J. J. P.; Waskell, L., Structure and Function of an NADPH-Cytochrome P450 Oxidoreductase in an Open Conformation Capable of Reducing Cytochrome P450. *Journal of Biological Chemistry* **2009,** 284, (17), 11374-11384.
94. Shen, A. L.; Porter, T. D.; Wilson, T. E.; Kasper, C. B., Structural analysis of the FMN binding domain of NADPH-cytochrome P-450 oxidoreductase by site-directed mutagenesis. *J Biol Chem* **1989,** 264, (13), 7584-9.
95. Shen, A.; Porter, T.; Wilson, T.; Kasper, C. B., Characterization of the Fmn Binding Domain of Nadph-Cytochrome-P-450 Oxidoreductase. *Faseb Journal* **1988,** 2, (4), A355-A355.
96. Esteves, F.; Campelo, D.; Gomes, B. C.; Urban, P.; Bozonnet, S.; Lautier, T.; Rueff, J.; Truan, G.; Kranendonk, M., The Role of the FMN-Domain of Human Cytochrome P450 Oxidoreductase in Its Promiscuous Interactions With Structurally Diverse Redox Partners. *Frontiers in Pharmacology* **2020,** 11, (299).
97. Vermilion, J. L.; Ballou, D. P.; Massey, V.; Coon, M. J., Separate roles for FMN and FAD in catalysis by liver microsomal NADPH-cytochrome P-450 reductase. *J Biol Chem* **1981,** 256, (1), 266-77.
98. Flück, C. E.; Pandey, A. V.; Huang, N.; Agrawal, V.; Miller, W. L., P450 oxidoreductase deficiency–a new form of congenital adrenal hyperplasia. *Endocr Dev* **2008,** 13, 67-81.
99. Reisch, N.; Idkowiak, J.; Hughes, B. A.; Ivison, H. E.; Abdul-Rahman, O. A.; Hendon, L. G.; Olney, A. H.; Nielsen, S.; Harrison, R.; Blair, E. M.; Dhir, V.; Krone, N.; Shackleton, C. H. L.; Arlt, W., Prenatal Diagnosis of Congenital Adrenal Hyperplasia Caused by P450 Oxidoreductase Deficiency. *J Clin Endocr Metab* **2013,** 98, (3), E528-E536.

 doi:10.20944/preprints202510.0422.v1

100. Krone, N.; Reisch, N.; Idkowiak, J.; Dhir, V.; Ivison, H. E.; Hughes, B. A.; Rose, I. T.; O'Neil, D. M.; Vijzelaar, R.; Smith, M. J.; MacDonald, F.; Cole, T. R.; Adolphs, N.; Barton, J. S.; Blair, E. M.; Braddock, S. R.; Collins, F.; Cragun, D. L.; Dattani, M. T.; Day, R.; Dougan, S.; Feist, M.; Gottschalk, M. E.; Gregory, J. W.; Haim, M.; Harrison, R.; Olney, A. H.; Hauffa, B. P.; Hindmarsh, P. C.; Hopkin, R. J.; Jira, P. E.; Kempers, M.; Kerstens, M. N.; Khalifa, M. M.; Kohler, B.; Maiter, D.; Nielsen, S.; O'Riordan, S. M.; Roth, C. L.; Shane, K. P.; Silink, M.; Stikkelbroeck, N. M. M. L.; Sweeney, E.; Szarras-Czapnik, M.; Waterson, J. R.; Williamson, L.; Hartmann, M. F.; Taylor, N. F.; Wudy, S. A.; Malunowicz, E. M.; Shackleton, C. H. L.; Arlt, W., Genotype-Phenotype Analysis in Congenital Adrenal Hyperplasia due to P450 Oxidoreductase Deficiency. *J Clin Endocr Metab* **2012,** 97, (2), E257-E267.
101. Ono, H.; Numakura, C.; Homma, K.; Hasegawa, T.; Tsutsumi, S.; Kato, F.; Fujisawa, Y.; Fukami, M.; Ogata, T., Longitudinal serum and urine steroid metabolite profiling in a 46,XY infant with prenatally identified POR deficiency. *Journal of Steroid Biochemistry and Molecular Biology* **2018,** 178, 177-184.
102. Saito, K.; Kawai, K.; Tatsumi, K.; Miyado, M.; Katsumi, M.; Nakamura, S.; Ishikawa, T.; Miyasaka, N.; Fukami, M., POR mutations as novel genetic causes of female infertility due to partial 17 alpha-hydroxylase deficiency. *Hum Reprod* **2017,** 32, 104-105.
103. Fukami, M.; Ogata, T., Cytochrome P450 oxidoreductase deficiency: rare congenital disorder leading to skeletal malformations and steroidogenic defects. *Pediatr Int* **2014,** 56, (6), 805-808.
104. Aigrain, L.; Pompon, D.; Morera, S.; Truan, G., Structure of the open conformation of a functional chimeric NADPH cytochrome P450 reductase. *EMBO Rep* **2009,** 10, (7), 742-7.
105. Miller, W. L.; Pandey, A. V.; Flück, C. E., Disordered Electron Transfer: New Forms of Defective Steroidogenesis and Mitochondriopathy. *The Journal of Clinical Endocrinology & Metabolism* **2025,** 110, (3), e574-e582.
106. Sahakitrungruang, T.; Huang, N. W.; Tee, M. K.; Agrawal, V.; Russell, W. E.; Crock, P.; Murphy, N.; Migeon, C. J.; Miller, W. L., Clinical, Genetic, and Enzymatic Characterization of P450 Oxidoreductase Deficiency in Four Patients. *J Clin Endocr Metab* **2009,** 94, (12), 4992-5000.